OPTICAL ABSORPTION OF PURE WATER IN THE BLUE AND ULTRAVIOLET

A Dissertation

by

ZHENG LU

Submitted to the Office of Graduate Studies of
Texas A&M University
in partial fulfillment of the requirements for the degree of

DOCTOR OF PHILOSOPHY

May 2006

Major Subject: Physics

OPTICAL ABSORPTION OF PURE WATER IN THE BLUE AND ULTRAVIOLET

A Dissertation

by

ZHENG LU

Submitted to the Office of Graduate Studies of
Texas A&M University
in partial fulfillment of the requirements for the degree of

DOCTOR OF PHILOSOPHY

Approved by:

Chair of Committee,	Edward S. Fry
Committee Members,	George W. Kattawar
	Robert A. Kenefick
	Ohannes Eknoyan
Head of Department,	Edward S. Fry

May 2006

Major Subject: Physics

ABSTRACT

Optical Absorption of Pure Water in the Blue and Ultraviolet. (May 2006)

Zheng Lu, B.S., Shandong University;

M.S., Nankai University

Chair of Advisory Committee: Dr. Edward S. Fry

The key feature of the Integrating Cavity Absorption Meter (ICAM) is that it produces an isotropic illumination of the liquid sample and thereby dramatically minimizes scattering effects. The ICAM can produce an effective optical path length up to several meters. As a consequence, it is capable of measuring absorption coefficients as low as 0.001 m^{-1}. The early version of the ICAM was used previously to measure the absorption spectrum of pure water over the 380-700 nm range. To extend its range into the ultraviolet, several modifications have been completed. The preliminary tests showed that the modified ICAM was able to measure the absorption of pure water for the wavelength down to 300 nm. After extensive experimental investigation and analysis, we found that the absorption of Spectralon$^{®}$ (the highly diffusive and reflective material used to build the ICAM) has a higher impact on measurements of absorption in the UV range than we had expected. Observations of high values for pure water absorption in the UV, specifically between 300 and 360 nm, are a consequence of absorption by the Spectralon$^{®}$. These results indicated that even more serious modifications were required (e.g. Spectralon$^{®}$ can not be used for a cavity in the UV). Consequently, we developed a new diffuse reflecting material and used fused silica powder (sub-micron level) sealed inside a quartz cell to replace the inner

Spectralon® cavity of the ICAM. The new data is in excellent agreement with the Pope and

Fry data (380-600 nm) and fills the gap between the 320 nm data of Quickenden and Irvin

and 380 nm data of Pope and Fry. We present definitive results for the absorption spectrum

of pure water between 300 and 600 nm.

To My Wife

ACKNOWLEDGMENTS

Thanks to my advisor, Dr. Edward S. Fry, for all the support, enlightening suggestions and great encouragement. I would like to thank all my committee members, Dr George W. Kattawar, Dr. Robert A. Kenefick and Dr. Ohannes Eknoyan for expertise, encouragement, helpful discussions and comments.

Special thanks to Shayna Sung for constantly helping me using the Spectrophotometer to measure the calibration dye solutions.

Thanks to the Machine Shop and Electronic Shop in the Physics Department, and the Glass Shop in Chemistry Department for their invaluable assistance.

 I reserve my final thanks to Xinmei Qu who is not only my wife, understanding and supporting me all the time, but also my colleague, sparing no efforts to help me in the absorption measurement and data analysis.

TABLE OF CONTENTS

LIST OF FIGURES

Page

Page

xiii

Page

LIST OF TABLES

CHAPTER I

INTRODUCTION

1.1 Optical Absorption of Water

The absorption and scattering characteristics are called inherent optical properties of natural water (including both seawater and inland water). Absorption and scattering are critical in determining the optical properties of the oceans; they have great applicability in designing *in situ* measurements and in remote sensing of ocean waters. Knowledge of the spectral absorption is essential to the understanding of radiative transfer in the oceanic water column. The profiles of optical absorption in the ocean are extremely important for tracking and understanding many of the physical processes in the ocean. In oceanography, the study of ocean color provides insight into the abundance and concentration of phytoplankton, sediments and dissolved organic compounds in the surface ocean waters. The resulting information can be used to investigate biological productivity, marine optical properties, interaction of winds and currents with ocean biology, and how human activities influence the oceanic enviroment. The spectral absorption of pure water provides vital input into the modeling of spectral reflectance that is important to ocean color studies.[1] It also provides a baseline for determining the diffuse attenuation coefficient and the absorption coefficient due to dissolved or suspended organic and biological materials.[2-4] The pure water absorption spectrum plays a very important role in many other scientific disciplines, e.g. biology, chemistry, meteorology, semiconductor processing, imaging, etc.

_____

This dissertation follows the style of Applied Optics.

The spectral absorption coefficient has been studied by a large number of research groups using a variety of techniques. There are several reviews that provide many pertinent references to the literature.[5-9] These references show notable inconsistencies due to experimental error or sample impurity. Consequently, there has been considerable uncertainty with regard to the correct values of the absorption coefficient of pure water in the visible and near-visible regions.

This confusion has been largely cleared up with the data obtained by Pope and Fry[10] using their prototype Integrating Cavity Absorption Meter (ICAM).[11,12] Their data provided a major advance in accuracy, and is highly reliable due to the many crosschecks and consistency tests.[13,14] In independent studies, this data are in excellent agreement with recent measurements of absorption coefficients for deep-sea ice,[15] and with those using a photothermal probe beam deflection technique.[16,17] The importance of this new data at wavelengths shorter than 500 nm is succinctly stated by Morel:[1] "Such a drastic revision (in the values of the absorption coefficient) is of considerable impact, in particular on the understanding of the optical properties of extremely pure oligotrophic, waters, which form a wide part of the world ocean. These new values, in the violet part of the spectrum, strongly suggest that the currently admitted absorption coefficients in the near-UV (400-300 nm) domain are likely to be also revised."

Based on present references, there is no truly reliable data in the 300-380 nm range. Quickenden and Irvin[18] have obtained what appear to be the most often referenced data in the 196-320 nm range, but there is no independent confirmation. Furthermore, in order to eliminate organic contaminants that absorb in the blue and ultraviolet, Quickenden and

Irvin used an oxidative purification process that involved extensive contact with quartz, sometimes at very high temperatures. In our experience high purity water samples that have been in extensive contact with quartz or glass have significantly increased absorption in the blue. With the ICAM we have been able to monitor this increase in absorption as a function of the storage time in quartz containers. The concern is further highlighted by the relatively large values for the absorption coefficient in the 390-450 nm range obtained by Litjens, Quickenden, and Freeman[19] using the similar oxidative purification process as Quickenden and Irvin did previously.

1.2 ICAM

Natural water has a narrow transmission window in the visible region of spectrum. In a large portion of this region (including both the blue and green spectrum) and in the UV-A part, the values of absorption coefficient are so low (< 0.2 m^{-1}) that it is difficult to measure them. Specifically, scattering effects interfer with absorption measurements. To overcome the problems of low absorption measurements in the presence of severe scattering effects, Elterman suggested the idea of integrating cavity spectroscopy[20]. Fry *et al.*[11,12] adopted this concept to develop the ICAM; excellent absorption data for pure water were obtained by using the ICAM. Mathematical Monte Carlo modeling shows that the operation of the ICAM is essentially unaffected by scattering,[11] in agreement with the experimental observations of Fry *et al.*[12]. Kirk[21] has also modeled the ICAM and has proposed a variant, the Point Source ICAM, or PSICAM. The key feature of the ICAM is that it produces an isotropic and homogeneous illumination of the liquid sample and thereby eliminates

scattering effects. To achieve this, the ICAM has a configuration shown in Fig. I-1. It consists of two concentric cylinderical integrating cavities, the outer cavity and the inner cavity, whose walls are made of a highly diffuse, reflective material with a relatively flat spectral response over most of the UV-VIS-NIR. The liquid sample is placed inside the inner cavity, which is surrounded by the outer cavity wall. Light is introduced into the space between the two cavities and creates a relatively diffuse and uniform light field as a consequence of multiple reflections due to high reflectivity of the walls. A small portion of light passes through the inner cavity wall, leading to an isotropic illumination, from which light is absorbed by the sample at a rate related to the absorption coefficient.
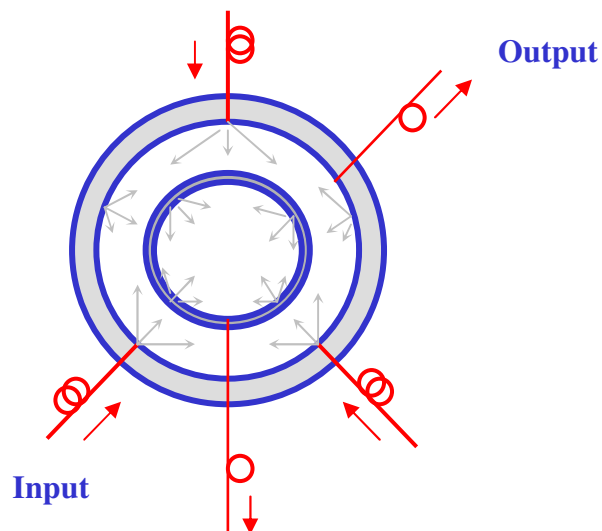
Figure I-1. Cross section of a generic ICAM

related to the absorption coefficient. Two optical fibers, located at the midpoint of each cavity wall, are used to sample the irradiance inside the inner cavity and the irradiance in the area between the inner and the outer cavity. By monitoring the change in irradiance

between the case when there is no sample inside the cavity (called Empty Cavity) and the case when the cavity is filled with sample (called Full Cavity), the relative absorption coefficient can be obtained. Similarly, by replacing the sample with calibration solutions whose absorption coefficients are accuately known, the absolute absorption coefficient can be determined.

There are two major advantages associated with the ICAM. First, the sample is isotropically illuminated so the measurement is independent of scattering effects. Second, due to the high reflectivity of cavity wall, the photons undergo many internal reflections before they are absorbed by the sample so the total effective optical path length can be up to sereral meters.[12,22] As a consequence, even very small absorption coefficients (as low as 0.001 m^{-1} level) can be measured with the ICAM. An example is the absorption spectrum of pure water measured by Pope and Fry.[10]

1.3 Objectives

The primary objective of this research effort is to modify the early version of the ICAM and to extend the measurements into the UV region. The data in the 300-400 nm range will fill a very important gap in available information. Other research goals are: to improve the accuracy in the absorption measurements at the minimum of pure water absorption; to investigate the apparent fact that contact of ultra-pure water with glass and quartz leads to increased absorption in the blue to near ultraviolet range; to study, build, and to test a long tubular form of integrating cavity with the objective of an *in situ* device that can directly measure both the absorption and scattering coefficient for natural waters.

CHAPTER II

BACKGROUND

2.1 Theory

Consider a liquid sample placed in an isotropic homogeneous light field. The power absorbed by the sample is independent of scattering effects and can be written as a linear function of the absorption coefficient,[10,12,22]

$$P_{abs} = 4\alpha V F_{out},$$ (2.1)

where V is the sample volume and F_{out} is the outwardly directed irradiance at the surface of the sample.

A form of more practical use is obtained by relating Eq. (2.1) to the generic model of the ICAM as shown in Fig. II-1. According to energy conservation, the power entering the sample volume V is equal to the power leaving the sample volume plus the power absorbed by the sample:

$$P_{in} = P_{out} + P_{abs}.$$ (2.2)

Combining this with Eq. (2.1) gives

$$P_{in} = P_{out} + 4\alpha V F_0,$$ (2.3)

where $F_0 = F_{out}$.

The power in is proportional to the irradiance F_1 in the outer cavity and the power out is proportional to the irradiance F_0 in the inner cavity. By introducing the proportionality constants K_1 and K_0, the energy conservation equation becomes

$$K_1 F_1 = K_0 F_0 + 4 \alpha V F_0. \tag{2.4}$$

As shown in Fig. II-1, the irradiances F_1 and F_0 are sampled by optical fibers and converted to voltage signals S_1 and S_0, respectively, by detectors D_1 and D_0. So Eq. (2.4) can be rewritten as

$$C_1 S_1 = C_0 S_0 + 4 \alpha V S_0 \tag{2.5}$$
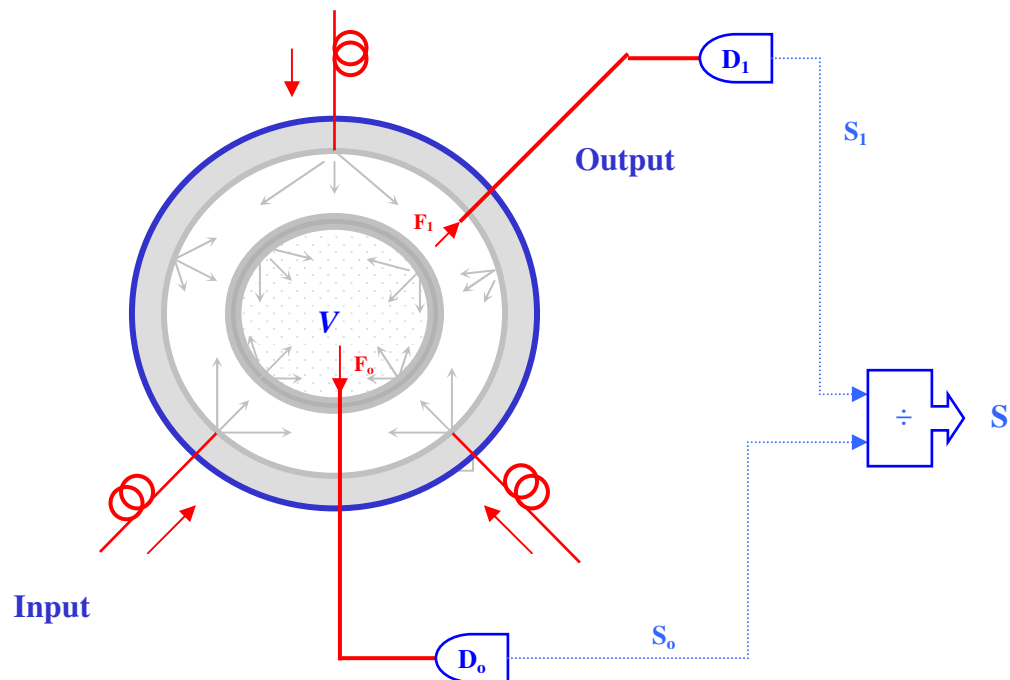
Figure II-1. Cross section of a generic model of the ICAM

Here K_1 and K_0 are replaced by new proportionality constants C_1 and C_0. To simplify this equation, dividing Eq. (2.5) by $C_1 S_0$ gives

$$\frac{S_1}{S_0} = \frac{C_0}{C_1} + \frac{4\alpha V}{C_1}. \tag{2.6}$$

Replacing S_1/S_0 by S (so called the ICAM signal) and replacing C_0/C_1 by C_0' leads to

$$S = \frac{4V}{C_1}\alpha + C_0'. \tag{2.7}$$

Solving for the absorption coefficient α gives

$$\alpha = \frac{C_1}{4V}(S - C_0') \equiv C_1'(S - C_0'). \tag{2.8}$$

This simple relation is the working equation for the ICAM.

2.2 Calibration Methods

The implementation of ICAM requires determination of C_1' and C_0', usually called the calibration constants. C_1' is difined as overall normalization constant and C_0' is the offset constant. Two partial derivatives derived from Eq. (2.7) and (2.8) will be particularly useful during calibration procedures:

$$\left.\frac{\partial S}{\partial V}\right|_\alpha = \frac{4}{C_1}\alpha, \tag{2.9}$$

$$\left.\frac{\partial \alpha}{\partial S}\right|_V = \frac{C_1}{4V} \equiv C_1', \tag{2.10}$$

For an ideal integrating cavity, C_1' and C_0' are constant numbers independent of α at fixed wavelength. It is straightforward to determine these constants. For the special case when there is no sample placed inside the inner cavity, α is just zero. Substituting $\alpha = 0$ into Eq. (2.8) simply gives $C_0' = S_E$. Here the signal S is denoted by the empty cavity signal S_E to be distinguished from the full cavity signal S_F, which is the signal in the case when the inner cavity is filled with a sample. Another calibration constant C_1' can be determined by measuring the signals for different calibration solutions whose absorption coefficients are accurately known, and then by determining the slope of the plot of α versus S (i.e., $\partial\alpha/\partial S$), see Eq. (2.10).

In practice, unfortunately, the determination of calibration constants is somewhat more complicated than for an ideal cavity. Fig. II-2 shows examples of the ICAM signal S as a function of sample volume V, $S(V)$ at three different wavelengths. Those data were taken from the experimental results with pure water using ICAM VERSION-II, the latest version of the ICAM that will be discussed in chapter V. A linear least-square fitting procedure is used to determine the intersection with the S axis. Fig. II-2(c) is a case closer to an ideal cavity: the S intersection is close to $S(V=0)$, which is just the empty cavity signal S_E; it should be equal to C_0' according to the relation $C_0' = S_E$. However, in the cases like Fig. II-2(a) and (b), the S intersections differ from $S(V=0)$ or S_E. The relation $C_0' = S_E$ for an ideal cavity is no longer accuate for a real ICAM.
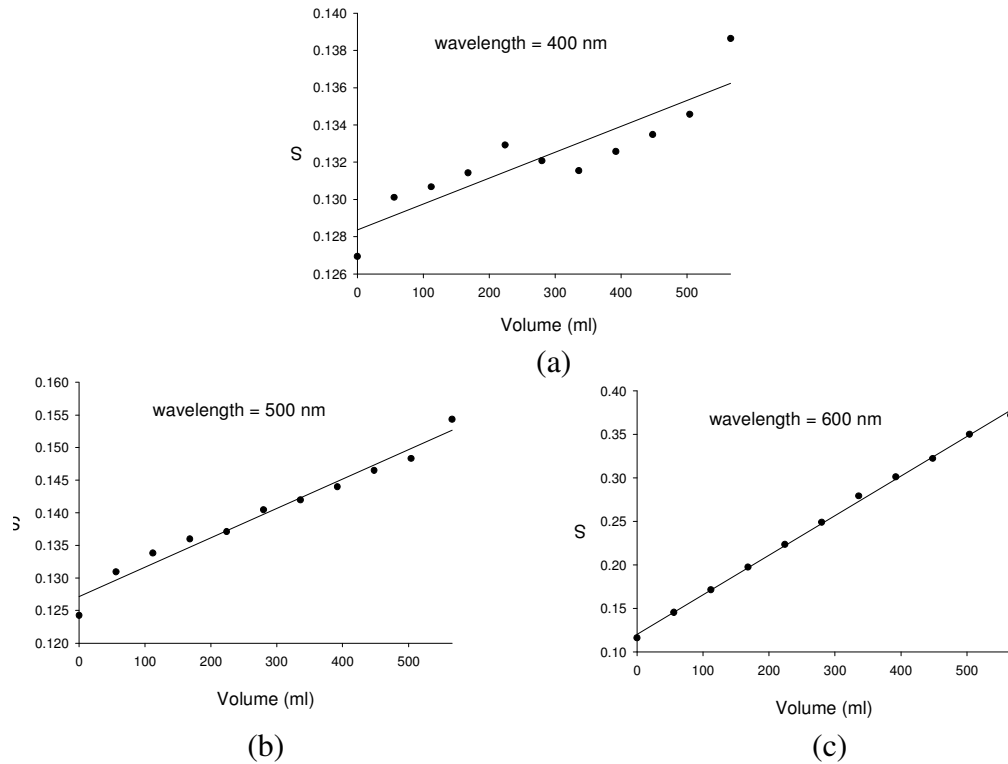
Figure II-2. Examples of the signal S as a function of the volume V at three wavelengths. Also shown is the linear least-square fit.

The complexity comes from several perturbations of the irradiance during measurement process. First, the irradiance is perturbed by leakage of optical power due to several holes in the cavity wall: for each cavity (outer or inner) there is a hole for the detector at midpoint; and two more significant holes at the top and bottom to allow the sample to flow through the cavity. Second, the index of refraction effects on outgoing irradiance F_0 in the vicinity of detector lead to systematic change from the empty cavity signal $S(0) \equiv S_E$, to the half full (approximatiely) cavity signal $S(280) \equiv S_H$, and the full cavity signal $S(566) \equiv S_F$.

Specifically, optical coupling to the fiber changes as the water level rises past the fiber monitoring F_0. All these perturbations lead to an effective sample volume V_{eff} that is different from the actual V. Furthermore, as the consequence of their effects on irradiance, the offset constant C_0' can depend on the sample absorption α that is related to the slope $\partial S/\partial V$. In order to calibrate the ICAM, this dependence must be identified and excluded. A working equation analogous to Eq. (2.8) has been developed together with new definitions of the two calibration constants.

2.2.1 Offset Calibration

This calibration prodedure is as following: the ICAM is filled with sequentially increasing volume of pure water; at each volume, S is measured and recorded at fixed wavelengths over the entire spectral range of interest; finally, at each wavelength S is plotted as a function of V. As characterized in Fig. II-3, there are three notable signal shifts. These systematic shits are caused by the index of refraction change when the liquid sample level approaches the midpoint of the inner cavity where the F_0 detector fiber is located, and by effects of the perturbation on the irradiance distributions at the bottom and top of the cavity. The shifts, $s_0(\lambda)$, $s_1(\lambda)$, and $s_2(\lambda)$ are designated the center shift, the cavity-empty shift, and the cavity-full shift. It should be emphasized that the liquid sample does not directly contact the cavity wall, rather, it is in a quartz cell in the inner cavity. The quartz cell has a total capacity of 566 ml. Since S_E, S_H, and S_F exhibit systematic deviations, these three data points are excluded during the fitting process. We define a fitting function of the form
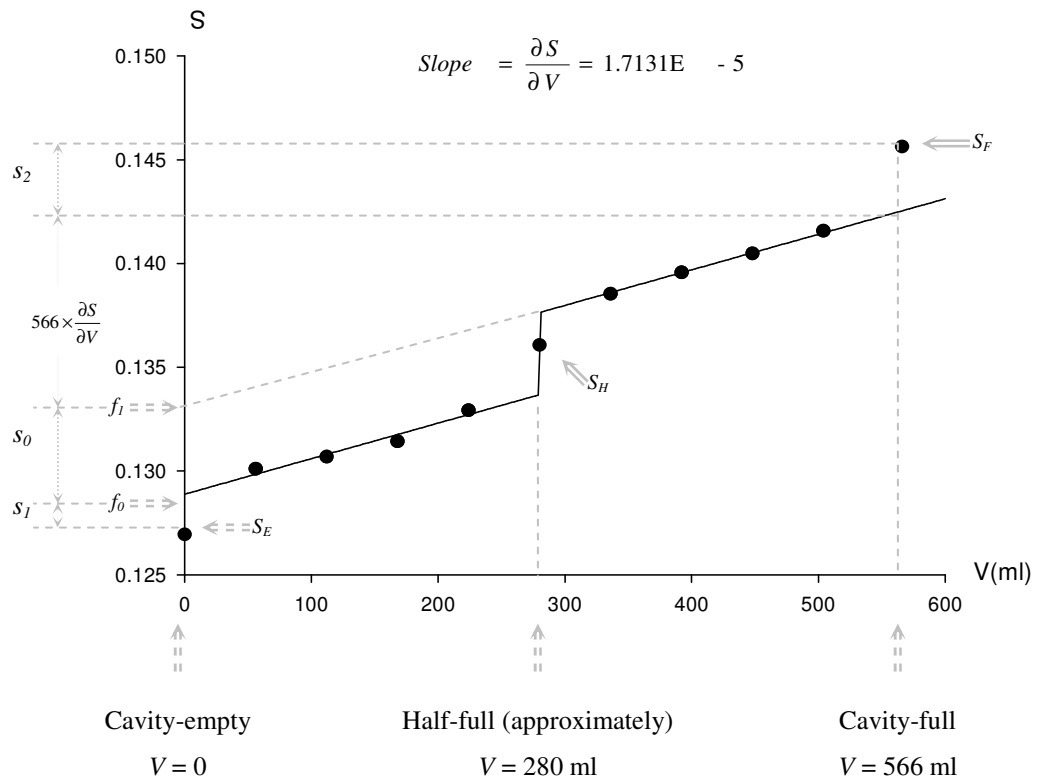
Figure II-3. Pictorial simulation of the $S(V)$ data showing the new linear fit, the definitions of three signal shifts (s_0, s_1, and s_2), and the slope $\partial S/\partial V$.

$$
\begin{aligned}
f(V) &= f_0 + \frac{\partial S}{\partial V}V & &\text{if} \quad V < 280 \ ml, \\
&= f_1 + \frac{\partial S}{\partial V}V & &\text{if} \quad V > 280 \ ml.
\end{aligned}
\tag{2.11}
$$

Here f_0 and f_1 are intercepts on the S axis corresponding to the two straight lines fitted to the $S(V)$ data (less the three points).

The standard measurement of an absorbing sample always involves first measuring a baseline with the cavity empty, S_E; and then measuring the signal S with the cavity filled with pure water. For an ideal cavity, simply using Eq. (2.8) we have

$$\alpha = \frac{C_1}{4V}(S_F - S_E).\tag{2.12}$$

For a practical ICAM, the three systematic signal shifts must be considered so Eq. (2.12) is rewritten as

$$\alpha = \frac{C_1}{4V}[(S_F - s_2) - (S_E + s_0 + s_1)].\tag{2.13}$$

To reduce the numbers of variables, we define a net offset

$$s(\lambda) = s_0(\lambda) + s_1(\lambda) + s_2(\lambda).\tag{2.14}$$

Substituting $s(\lambda)$ into Eq. (2.13) gives

$$\alpha = \frac{C_1}{4V}(S_F - S_E - s).\tag{2.15}$$

Fig. II-3 indicates a more practical equation to calculate the net offset:

$$\begin{aligned}
s(\lambda) &= S_F - S_E - V\frac{\partial S}{\partial V}\\
&= S_F - S_E - 566 \times \frac{\partial S}{\partial V}.
\end{aligned}\tag{2.16}$$

Replacing the $\partial S/\partial V$ by using Eq. (2.9) we have

$$s\,(\lambda) = S_F - S_E - 566 \times \frac{4}{C_1}\,\alpha, \tag{2.17}$$

which shows that the net offset $s(\lambda)$ depends on the absorption coefficient α as expected from the discussion at the beginning of this section. This dependence must be isolated to calibrate the ICAM. We define a general function

$$s\,(\lambda) = k_1 + k_2\,\lambda + (k_3 + k_4\,\lambda)\,\frac{\partial S}{\partial V}, \tag{2.18}$$

where we assume a simple linear dependence on wavelength λ combined with a linear dependence on slope $\partial S/\partial V$ for $s(\lambda)$. Coefficients k_i ($i = 1,2,3,4$) are determined by a least-squares fit to the $s(\lambda)$ data which are directly evaluated from the experimental data $S(V)$ using Eq. (2.16).

Substituting Eq. (2.18) into Eq. (2.16) gives

$$\begin{aligned}
\alpha &= \frac{C_1}{4V}\left[\,S - S_E - k_1 - k_2\,\lambda - (k_3 + k_4\,\lambda)\frac{\partial S}{\partial V}\,\right] \\
&= \frac{C_1}{4V}\left[\,S - S_E - k_1 - k_2\,\lambda - (k_3 + k_4\,\lambda)\frac{4\alpha}{C_1}\,\right].
\end{aligned} \tag{2.19}$$

Solving for α gives the final working equation for our experimental realization of ICAM:

$$\alpha = C_1''\,(S_F - S_E - C_0''). \tag{2.20}$$

Where the two new calibrtion constants for normalization and offset are

$$C_1" \ = \ \frac{C_1}{4(V + k_3 + k_4\,\lambda)}\,, \tag{2.21}$$

$$C_0" \ = \ k_1 + k_2\,\lambda. \tag{2.22}$$

$C_1"$ and $C_0"$ are completely independent of absorption coefficient α. It should be noted that $C_0"$ is evaluated in practice via Eq. (2.22), while $C_1"$ is determined as discussed in the following section.

2.2.2 Normalization Calibration

This calibration involves the measurement of reference samples of accurately known absorption coefficients. Reference samples were made by dissolving dyes in pure water. During this calibration process, the ICAM output signal S_F for dye solution consists of the signal due to the dye itself (S_{dye}) and the signal due to the pure water solvent ($S_{pure\ water}$). In order to use ICAM to measure the pure water absorption, $S_{pure\ water}$ must be isolated.

Starting with the simple relation

$$S_{solution} \ = \ S_{dye} + S_{pure\ water}. \tag{2.23}$$

From Eq. (2.20), for dye solution we have

$$\alpha_{dye} + \alpha_{pure\ water} \ = \ C_1" \ (\ S_{solution} - S_E - C_0"\ ). \tag{2.24}$$

Similarly, for pure water solvent we have

$$\alpha_{pure\ water} = C_1" \ (S_{pure\ water} - S_E - C_0").$$

(2.25)

Eq. (2.24) minus Eq. (2.25) gives

$$\alpha_{dye} = C_1" \ (S_{solution} - S_{pure\ water}).$$

$$= C_1" \ S_{dye}$$

(2.26)

In analogy with Eq. (2.10), the normalization constant $C_1"$ can be written as

$$C_1" = \frac{\partial \alpha_{dye}}{\partial S_{dye}}.$$

(2.27)

The calibration procedure is as following: a pure water sample and a series of reference dye solutions of accurately known absorption coefficients are prepared; the ICAM is filled with these samples starting with pure water and then samples with sequentially higher absorption; for each sample, S is measured and recorded at the same wavelengths as in the offset calibration process; the pure water sample signal $S_{pure\ water}$ is subtracted from the signal $S_{solution}$ for each dye solution to obtain S_{dye} ($S_{dye} = S_{solution} - S_{pure\ water}$, Eq.(2.23)); finally, at each wavelength, S_{dye} is plotted as a function of the corresponding α_{dye}. Fig. II-4 shows examples of the signal S_{dye} as a function of the absorption coefficient α_{dye}, $\alpha(S)$ at three different wavelengths. These data are taken from experimental results using ICAM

VERSION-II. A linear least-square fitting procedure is used to determine the slope of the plot of $\alpha(S)$, i.e., the C_1".
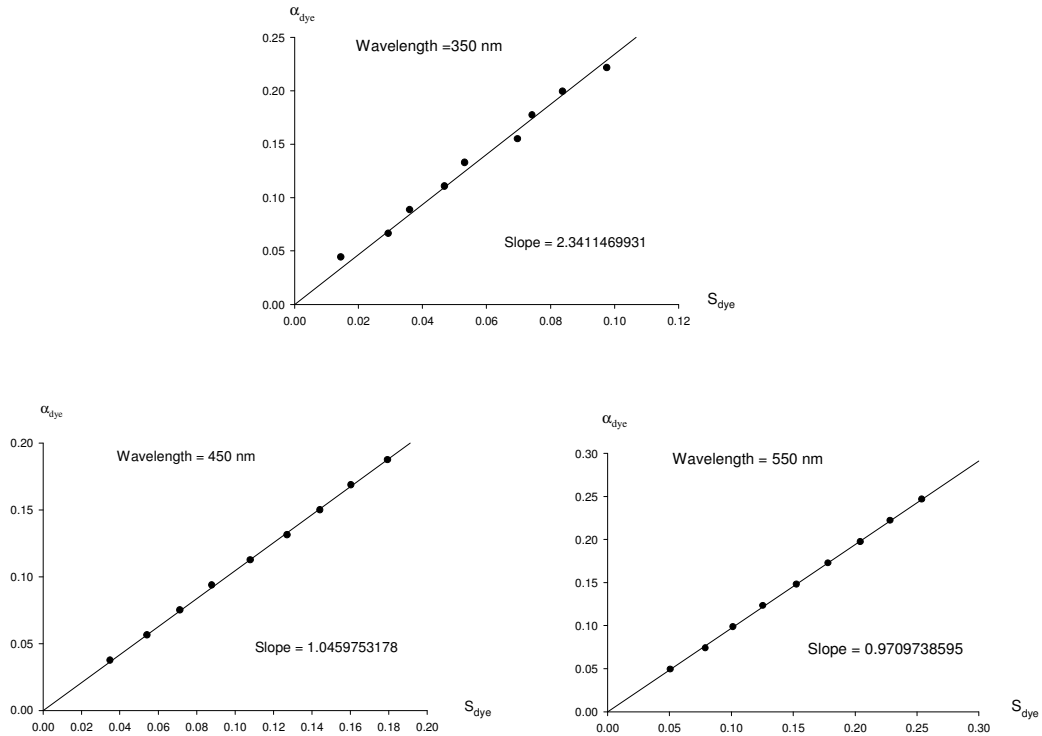
Figure II-4. Examples of the absorption α_{dye} as a function of the signal S_{dye} at three wavelengths. Also shown is the linear least-square fit and the slope $\partial\alpha/\partial S \equiv C_1$".

CHAPTER III

PURE WATER

3.1 Water Purification

Water is the most widely used laboratory chemical. The definitions of pure water are various depending on the applications. To specify the purity of the water, many standards are published by the professional organizations such as the Ad Hoc Committee for Laboratory Reagent-Grade Water Standards (Ad Hoc), the American Chemical Society (ACS), the American Society for Testing and Materials (ASTM), the College of American Pathologists (CAP), the International Organization for Standardization (ISO), the National Committee for Clinical Laboratory Standards (NCCLS) and the United States Phamacopeial Convention, Inc (USP). These standards are based on factors such as electrical resistance, metal ion content, and organic or microbial contaminants present in water. In this research study we are interested in "optical pure" water. The "absolutely pure" water is non-existent since ultrapure water leaches contaminants from its enviroment and is sometimes refered to "hungry" water.[23]

Usually, water with a resistivity of 18 megohms-cm at 25°C (the minimum limit of ASTM Type-I water) is defined as Type-I reagent grade water. Type-II analytical grade water is defined as having at least 1 megohm-cm resistivity. However, to only measure resistivity is inadequate. Water at the theoretically pure limit of 18.2 megohm-cm may still contain high concentrations of neutral organic contaminants which may adversely affect analytical

methods and cause analyses to fail. [24] The existence of organic matter will especially increase the absorption in the ultraviolet region.[25]

Water purification methods include distillation, active carbon adsorption, microporous membrane filtration, reverse osmosis (RO), electrodeionisation, UV treatment, and ultrafiltration. Each method has advantages and disadvantages. For instance, water triply distilled in quartz may still have some organics with low boiling points; the organic and microbial contaminants in water that has been treated with ion exchange can be killed and removed with ozone, UV, ultrafiltration, etc., but these steps can reduce the resistivity of the water somewhat.[26] Currently, most commercial systems are using a combination of these methods to generate ultrapure ionic-free/ organic-free water.

The pure water samples used in this project are from a Millipore water purification system,[27] which consists of three subsystems: Elix 10, 60 litres polyethylene reservoir, and Milli-Q with A10 TOC option, as shown in Fig. III-1.

Elix 10 produces Type-II quality water from potable tap water by combining several purification technologies. Tap water initially passes through a Progard[TM] pretreatment pack, which is designed to remove particles and free chlorine from the feed water. In addition, it helps to prevent mineral scaling in hard water areas. The water is pressurized with a pump and then is purified by reverse osmosis (RO) to generate intermediate quality water. Next, the RO product water passes through an electrodeionisation (E.D.I.) module to reduce levels of organic and mineral contaminants. The typical resistivity of Elix 10 product water is 10-15 MΩ-cm and the total organic carbon (TOC) is less than 30 μg / litre (ppb).

A 60 litre polyethylene reservoir is used for temporary storage of Elix 10 product water. On the top there is a vent filter used to filter any air entering the reservoir. An overflow tube is connected between the reservoir and a checkvalve. The checkvalve prevents air from entering the reservoir through the overflow tubing. A water level sensor is installed to display the amount of water inside the reservoir. For convenience, a valve is located on the front of the reservoir to be used to fill beakers or other containers with water directly from the reservoir. It is suggested that the reservoir should be drained if it is not used for over one week.

A. Progard pretreatment pack
B. Booster pump
C. Reverse osmosis (RO) cartridge
D. E.D.I. module
E. 60 L polyethylene reservoir
F. Pump
G. Q-Gard pack
H. UV lamp
I. Quantum ultra-pure cartridge
J. Ultra-filtration cartridge
K. A10 TOC monitor
L. 0.22 μm final filter
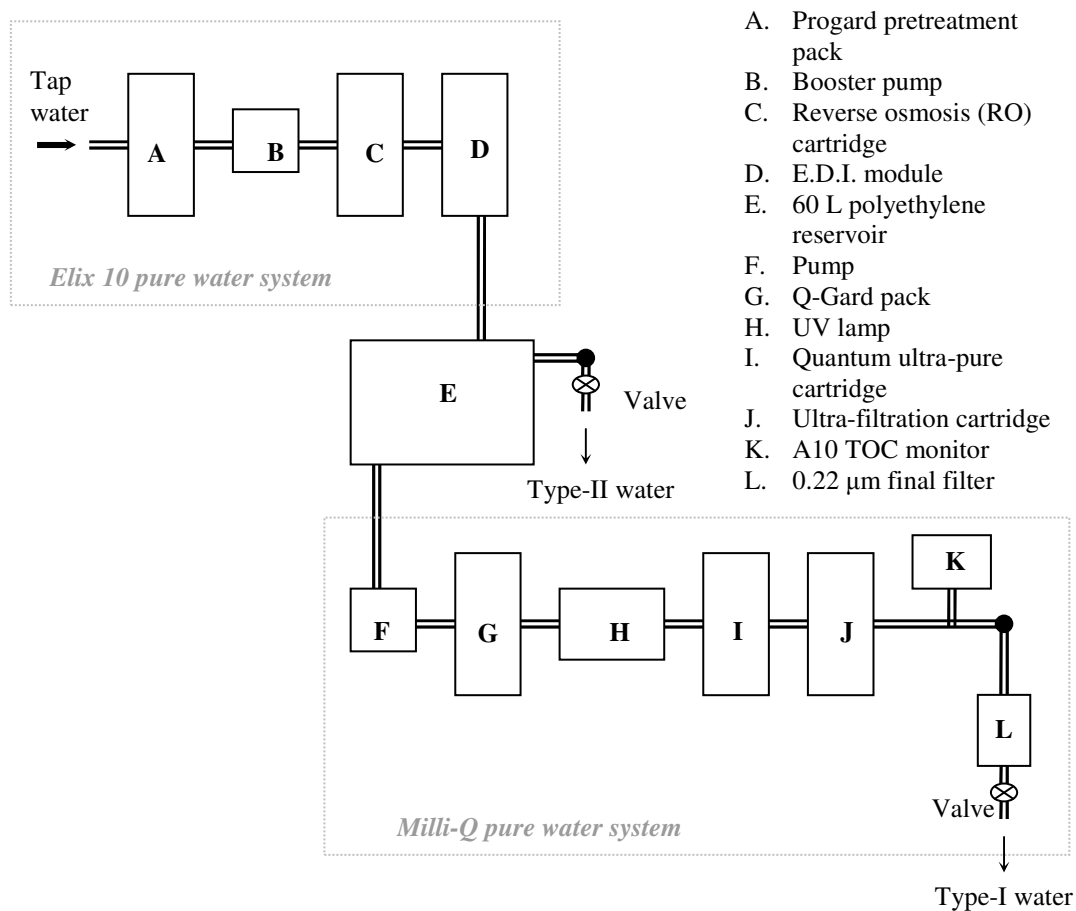
Figure III-1. Block diagram of the Millipore water purification system

The Milli-Q system is used as a final water purification stage. The feedwater comes from Elix 10 product water temporarily stored in the 60 litre reservoir. It produces water of Type-I quality, which is equal to or better than ASTM, CAP and NCCLS Type-I water quality standards. Pre-treated water enters the system and is pumped through the Q-Gard cartridge for an initial purification. Then the water is exposed to UV light at both 185 and 254 nm to oxidise organic compounds and to kill bacteria. The function of the Quantum cartridge is to remove trace ions and oxidation by-products produced by the action of the UV light. Purified water then passes through an Ultrafiltration (UF) module. The UF module acts as a barrier to colloids, particles and organic molecules with a molecular weight greater than 5000 Daltons. A manual 3-way valve directs ultrapure water through a final 0.22 μm membrane filter so that any particles or bacteria greater than 0.22 μm will be removed. An A10 TOC monitor is installed to measure the sample of ultrapure water to determine trace organic levels. This special feature makes real-time organic content monitoring a reality.

Unless otherwise noted, references to pure water in this dissertation refer to Millipore Type-I ultrapure water with the specifications: the resistivity is consistently 18.2 MΩ-cm and the total organic carbon (TOC) is from 3 to 4 μg / litre (3-4 ppb).

3.2 Sample Preparation

During preparation for an absorption measurement, all the glass or quartz containers, tubings, valves, and the ICAM sample cell are thoroughly washed with an acid cleaning solution,[28,29] that is made by dissolving potassium dichromate in Type-II water and then

mixing with sulfuric acid. The acid cleaning procedure is followed by rinsing 6-8 times with Type-II water followed by rinsing 4-6 times with Type-I water. Finally, high purity Nitrogen gas is used for blow drying.

In the measurement process, all pure water samples are drawn from Millipore system directly into the ICAM without any intermediate storage. This real-time feature minimizes time and possible contamination during sample delievery.

CHAPTER IV

ICAM VERSION-I

4.1 System Overview

In order to extend the measurement range of the ICAM (previously developed by Dr. Pope for his dissertation research[22] and later on improved by Liqiu Cui for her master thesis[23]) into the ultraviolet, several modifications have been done. The modified ICAM was named ICAM VERSION-I.
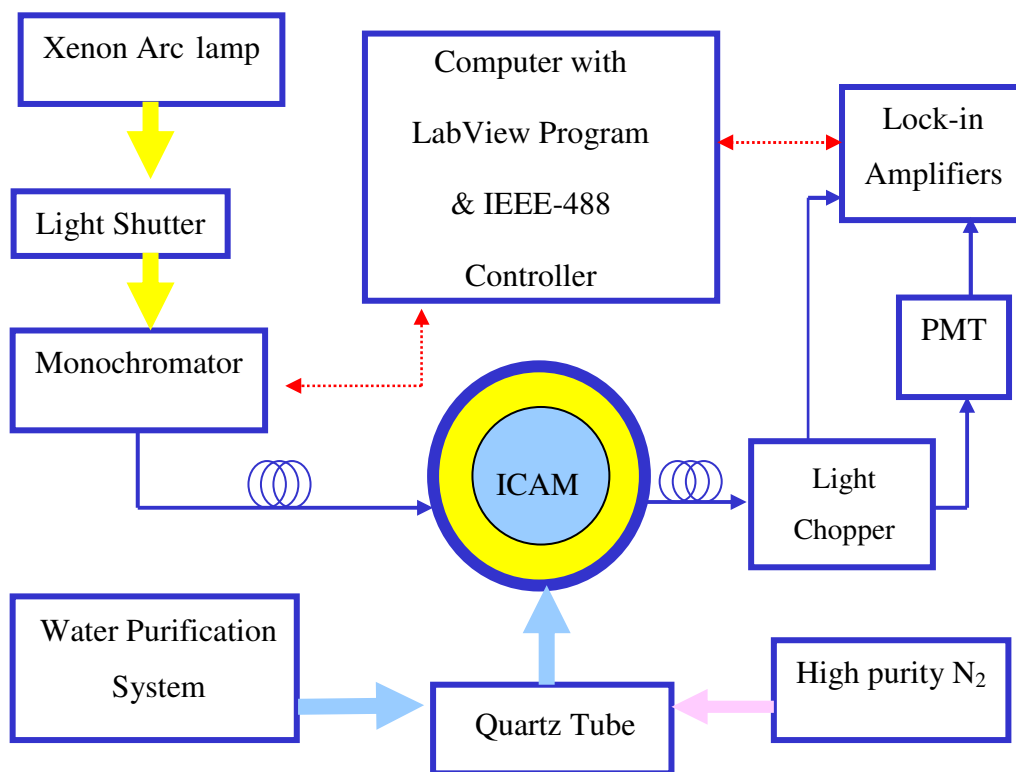
Figure IV-1. Block diagram of the ICAM VERSION-I.

All the optics were changed to make them UV compatible, including the Xenon arc lamp, monochromator, input fibers to the integrating cavity, and the sampling/detection fibers. A new water purification system, Millipore Elix10 combined with Gradient A10, was installed close to the ICAM apparatus. This new system simplifies the sample handling procedures; it directly provides fresh purified water samples without transfers between containers. To exclude oxygen and other contaminants, a new sample delivery system was implemented so that pure water samples only come in contact with quartz and are always sealed by high purity nitrogen gas (99.998%) during the measurements. Figure IV-1 shows a block diagram of the ICAM VERSION-I.

4.2 Apparatus

4.2.1 Illumination System

The arc lamp is the light source for the ICAM. Two different Oriel lamp systems have been used for the absorption measurement. The low power lamp system consists of an Oriel 6255 150 W ozone free xenon lamp, an Oriel 66005 lamp housing, and an Oriel 68700 200 W lamp power supply. An Oriel 6214 liquid fitter is mounted between a 3-inch *f* /0.7 Aspherab® UV grade fused silica condenser and a 3-inch *f* /3.0 fused silica secondary focusing lens. The liquid water filter is used to remove undesired infrared radiation.[30] It uses a fused silica window to transmit down to 250 nm and is filled with Type-I pure water. It also has an external chamber for circulation of cooling water supplied by the university chilled water system. The high power lamp system was introduced to gain more power in the UV, especially for measurements below 300 nm. It consists of an Oriel 6269 1000 W

xenon lamp, an Oriel 66923 lamp housing, and an Oriel 68920 1000 W lamp power supply. To reduce hazardous ozone, an Oriel 66087 ozone eater is required whenever the lamp is ignited. As with the low power system, an Oriel 6227 liquid water filter is used to remove infrared radiation. Unfortunately, the liquid fitlter alone was not sufficient to ensure the monochromator and the optical shutter against damage caused by exposure to the high power radiation. For experiments over a short period of time, a 3-inch CVI UR-3 UV reflecting mirror operating at 45º incident angle was used. The mirror transmits most of the red and IR to an air-cooled heatsink and reflects the shorter wavelength radiation into the monochromator.[31] For experiments over longer period of time, we specifically designed a prism with a 30º apex angle that provides sufficient wavelength dispersing to avoid optical damage at the focal points. The prism is mounted on a translation stage. We adjust the position of the stage to ensure the desired spectral region is forcused on the entrance slit of the monochromator. The rest of the light is blocked by an aperture. Fig. IV-2 shows a top view of experimental set-up for the prism. The body of prism is stainless steel. The two windows are 3-inch Esco S1-UV grade fused silica square plates. The cell is filled with Type-I pure water which served as both the prism medium for dispersing the light and as an absorber for removing the IR. A hole was drilled through the entire prism body and was connected to the university chilled water system. Cooling water first passes through the prism and then through a Lytron 6110G1SB liquid-to-air heat exchanger that is mounted on the lamp housing to cool the air flowing to the ozone eater.
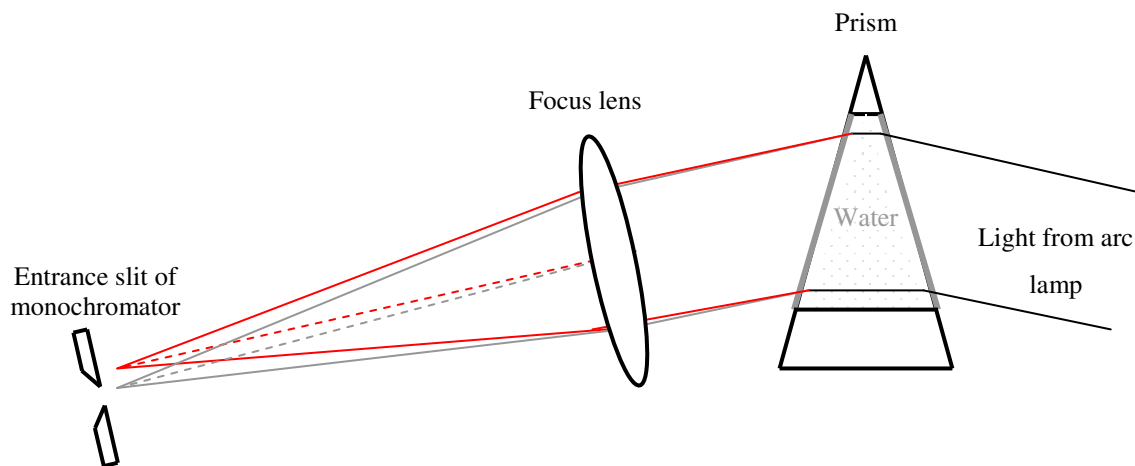
Figure IV-2. Top view of experimental set-up for the dispersing prism.

The light Shield is made of black corrugated PVC pipe. It shields the beam between the arc lamp and the optical shutter from dust and stray light.

The shutter is used to control the light entering the monochromator. A Copal DC-494 plunger shutter with a 30 mm diameter, 5 blade assembly is attached to the alluminum cover plate in front of the entrance slit of the monochromator. Closing this shutter allows measurement of the ICAM background signal due to PMT dark current and stray light. The shutter is powered by a DC 24 V plug-top transformer, which is controlled by an HP 6214A power supply. The shutter defaults to close when power is off.

The monochromator is a CVI Digikrom 240 classical Czerny-Turner monochromator with a 240 mm focal length and an effective aperture ratio of $f / 3.9$.[32] It can be controlled either by a control module through an RS-232C serial port, or by a computer through a GPIB (IEEE 488) interface. Typically, the former control mode is used for testing or quick

adjustment and the latter is the primary instrument control during absorption measurements. Digikrom 240 has a reversible, two-grating mount with two 1200 grove/mm gratings. The gratings are designated as #1 and #2 on the LCD of the control module. The peak transmissions of grating #1 and #2 are at 500 nm and 330 nm respectively. When continuously scanning from UV to IR, the grating must be changed from #2 to #1 at 620 nm. The reciprocal linear dispersion of the Digikrom 240 is 3.2 nm/mm and the spectral resolution is 0.06 nm with a 20 micron slit width. The optics inside the monochromator was coated with UV protected aluminum (PAUV).[33]

Input Fiber Assembly consists of six 1.5 m long silica-core, silica-clad optical fibers with 600 μm core diameter and 1.0 mm cladding diameter. Each fiber is shielded in furcation tubing (protective cable). This custom-made assembly from C Technologies, Inc.[22] is used to couple the light from the monochromator into the integrating cavity. At the input end the six fibers are arranged in a linear array and embedded in an aluminum ferrule, which is secured in a transparent Plexiglas block by a set screw. The orientation of the linear fiber array with respect to the exit slit, and the distance between the fiber and the exit slit can be adjusted and locked with the set screw. The Plexiglas block is mounted on a Newport X-Y translation stage attached to the cover plate in front of the exit slit of the monochromator; it is used to adjust the transverse position of the fiber relative to the exit slit. At the output end each fiber terminates in an aluminum ferrule for protection. The output end of each fiber extends about 1.3 cm beyond from the ferrule and through a 1 mm I.D. hypodermic tube. All the fiber ends are polished by Thorlabs polishing films (5 μm film followed by 3 μm and 1 μm films).

4.2.2 Integrating Cavity Assembly

The integrating cavity assembly is the critical part of the ICAM. It consits of two concentric integrating cavities and a Heraeus Suprasil quartz sample cell with inlet and outlet quartz tubes. The entire assembly is in a black light-tight Plexiglas box to shield it from external light sources. The box has ports for both inlet and outlet tubes, for the six input fibers (three at the top and three at bottom respectively), and for the two detector fibers described later in this section. All ports are sealed with black electrical tape. Fig. IV-3 shows cross sections of the integrating cavity assembly.

In Fig. IV-3 (b), viewed along the Z axis, the outer cavity has a hexagonal cross section with 107 mm between the inside faces. Its wall is made of six interlocking Spectralon® plates 12.7 mm thick and 254 mm high. Two 19 mm holes are drilled in the wall to mount the detectors. The outer cavity is closed by two 12.7 mm thick Spectralon® end caps. Each hexagonal cap has a 19 mm center hole for the sample cell inlet or outlet tube, and three 2 mm holes for the input fibers. The caps have three holes, 120º apart on a 113 mm diameter circle; on one cap they are offset by 60º with respect to those in the other cap.

Ferrule

Outer cavity
wall

F_0 detector fiber

Inner cavity
wall

Z

X

Input fibers

Quartz sample cell

Input fiber

(a)
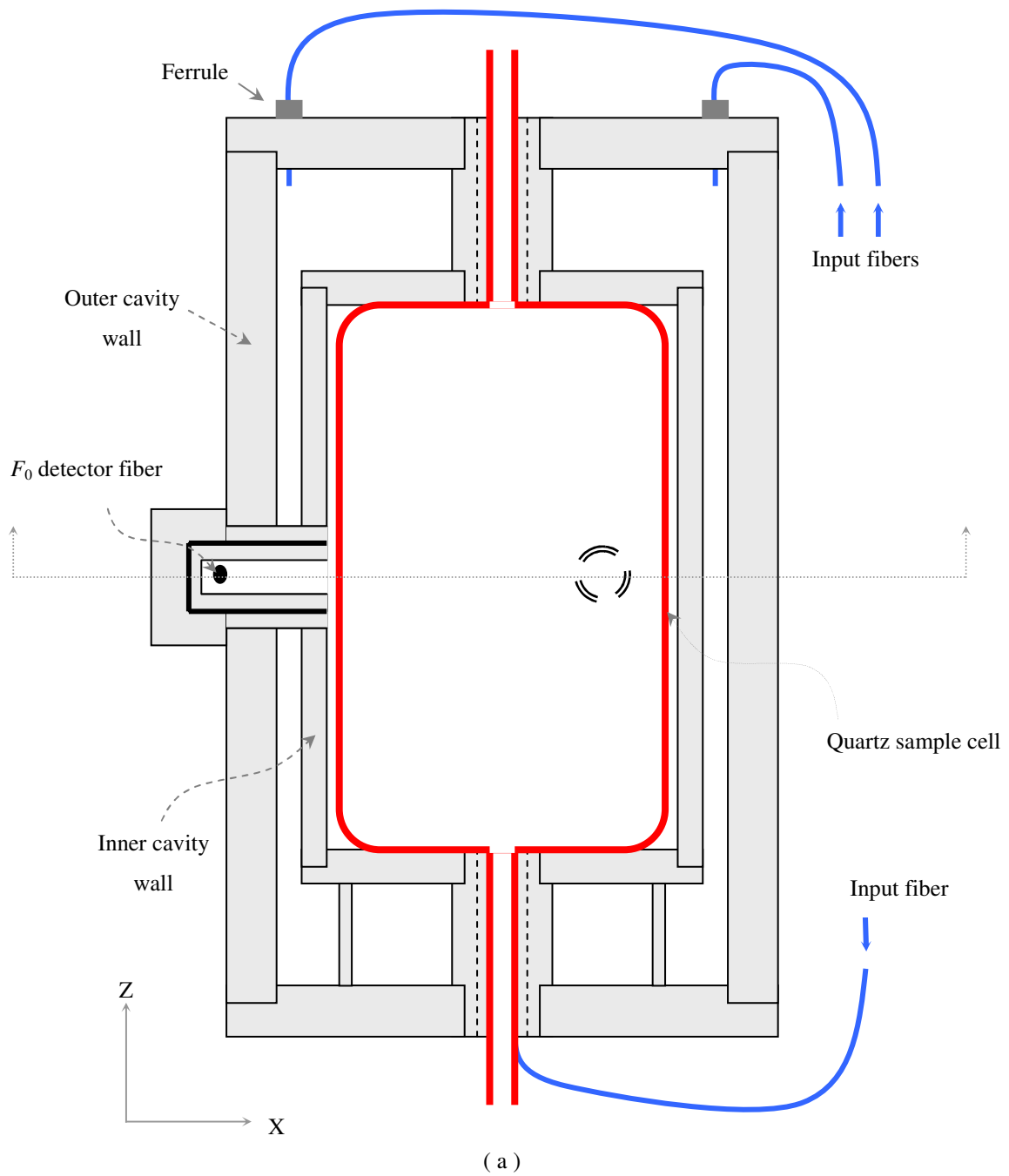
Figure IV-3. Cross section of the integrating cavity assembly
(a) perpendicular to Y axis and (b) perpendicular to Z axis.
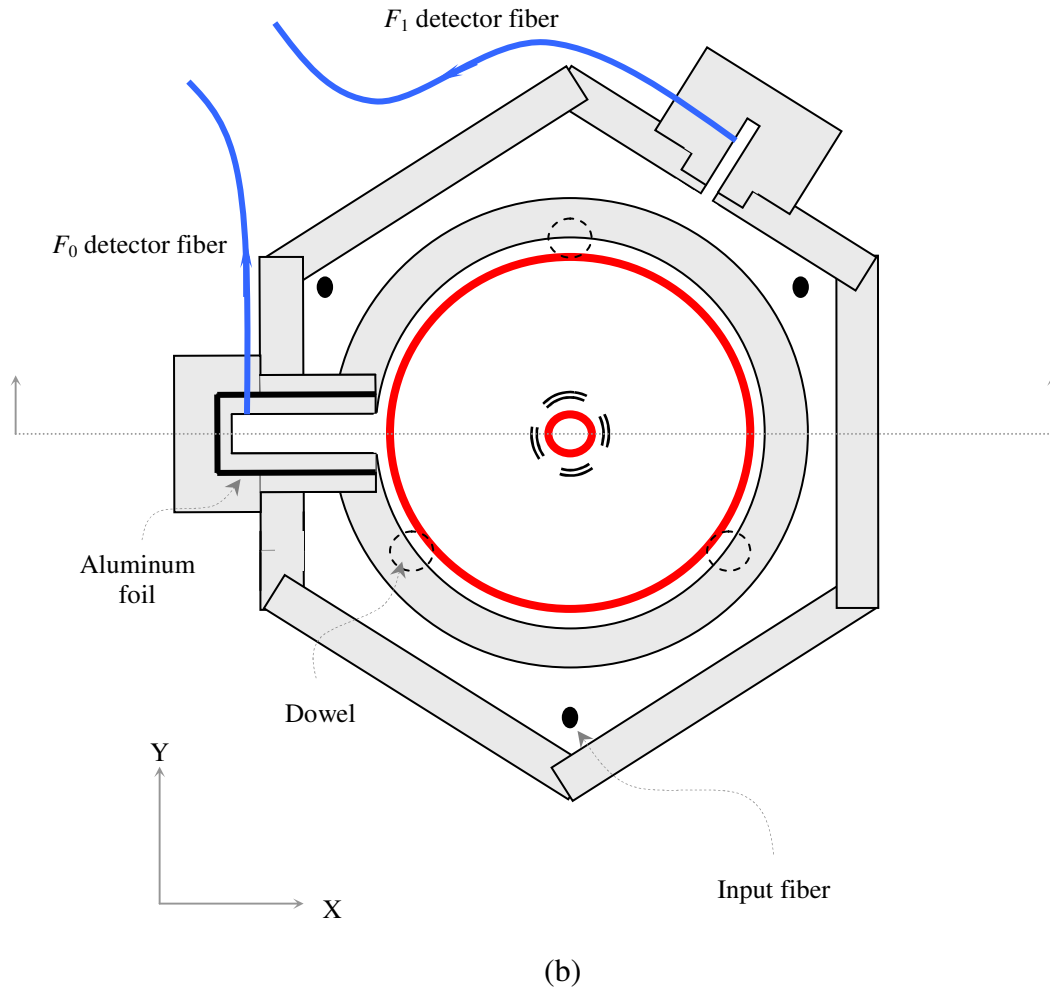
Figure IV-3. Continued.

The inner cavity is a 151 mm high Spectralon® cylinder with a 101.6 mm O.D., an 89 mm I.D., and two round Spectralon® end caps. Each end cap is 12.7 mm thick with a 19 mm hole in the center. The inner cavity is held at the midpoint of the outer cavity by Spectralon® tubes at the center and three additional Spectralon® dowels symmetrically

located on a 92 mm diameter circle at each end. The center tubes are 61 mm long with a 25.4 mm O.D. and a 12.5 mm I.D.. The dowels are 44 mm long and 9.5 mm diameter; the three of them at one end are offset by 60º with respect to those at the other end. The quartz sample cell lining the inner cavity has a 566 ml total capacity. The outside diameter of the quartz cell is slightly smaller than the inside diameter of the inner cavity. Its main body is 135 mm long and tapers into a 125 mm long, 7 mm O.D., 5 mm I.D. quartz tube at each end. The outside surface of main body is heavily frosted in order to minimize specular reflection effects when light enters the cell through the quartz-air interface.[12]

Input light is introduced into the outer cavity through the six fibers from the input fiber assembly. Three aluminum ferrules with hypodermic tube extensions that shield the fiber tips pass through each end of the black Plexiglas box. The hypodermic tubes then pass through the end caps and terminate in the outer cavity.

The light inside the cavities are sampled by detector fibers extending through two Spectralon® cups, as shown in Fig. IV-3 (b). As described in Chapter II, the outward irradiance incident on the inside wall of the outer cavity is designated as F_1 and the outward irradiance incident on the inside wall of the inner cavity is designated as F_0. Each irradiance is sampled by the corresponding detector fiber in the Spectralon® cups. The two cups are located at the midpoint of the Z axis and are separated by 120º in the X-Y plane. A 2 mm diameter port is drilled near the back of each cup for the detector fibers. These two ports are sealed with black insulating tape after the detector fibers are inserted. The first cup with the irradiance F_1 detecting fiber has a 19 mm O.D. and a 4.8 mm I.D.; it terminates on the inside wall of the outer cavity. The second cup is 19 mm O.D. and 12.5 mm I.D. it is

inserted through the outer cavity wall and terminates in the wall of the inner cavity as shown in Fig. IV-III. Another Spectralon® cup with 12.5 mm O.D. and 6 mm I.D. is pressed into the second cup with an aluminum foil embeded between them to prevent cross talk between the two irradiances F_1 and F_0. The irradiance F_0 detecting fiber extends into this cup.

Spectralon® is the material used to build both the outer and inner cavities of the ICAM. This diffuse reflectance material exhibits relatively flat spectral distribution and gives the highest diffuse reflectance of any previously known material or coating over the UV-VIS-NIR region of the spectrum.[34] In each case, reflection and transmission, Spectralon® is almost perfectly lambertian. The reflectance is generally >99% over a range from 400 to 1500 nm and >95% from 250 to 2500 nm. Values of its reflectivity[35] are shown in Table IV-1 and are plotted in Fig. IV-4. The reflectance of Spectralon® also depends on it thickness as shown in Table IV-2[36] and are plotted in Fig. IV-5. Spectralon®'s highly diffuse and highly reflective performance is the key to realize the isotropic illumination of the water sample inside the inner cavity.

Table IV-1. Typical 8˚ hemispherical reflectance for Spectralon® SRS-99

Wavelength (nm)	Reflectance
250	0.973
300	0.984
400	0.991
500	0.991
600	0.992
700	0.992
800	0.991
900	0.991
1000	0.993
1100	0.993
1200	0.992
1300	0.993

Wavelength (nm)	Reflectance
1400	0.991
1500	0.992
1600	0.992
1700	0.988
1800	0.989
1900	0.981
2000	0.976
2100	0.953
2200	0.973
2300	0.972
2400	0.955
2500	0.960
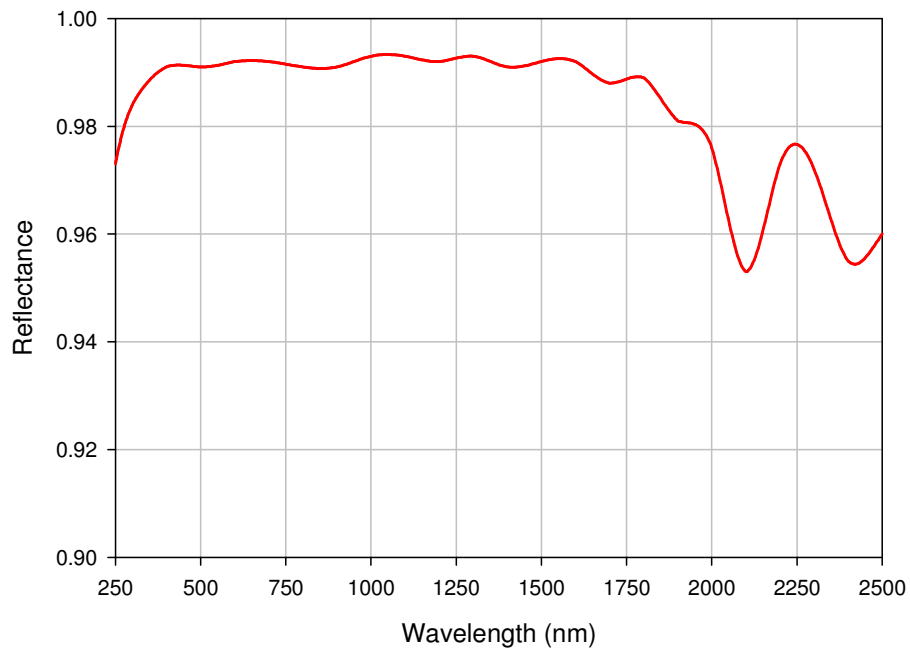
Figure IV-4 Typical 8° hemispherical reflectance for Spectralon® SRS-99

(Labsphere, Inc.).

Table IV-2. Reflectance versus thickness for Spectralon® material

Wavelength (nm)	Thickness (mm)						
	1	2	3	4	5	6	7
325	0.934	0.959	0.970	0.973	0.988	0.985	0.985
450	0.937	0.962	0.973	0.977	0.992	0.991	0.991
555	0.933	0.960	0.972	0.976	0.989	0.989	0.990
720	0.928	0.958	0.970	0.976	0.988	0.987	0.989
850	0.922	0.956	0.969	0.976	0.985	0.986	0.987
1060	0.916	0.954	0.968	0.974	0.986	0.986	0.988
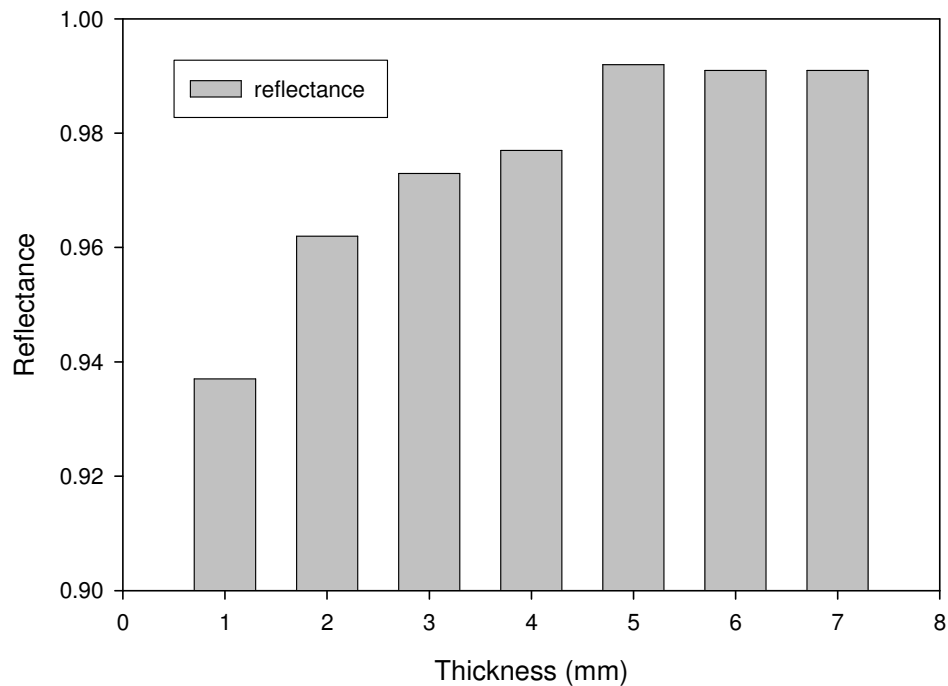
Figure IV-5. Reflectance versus thickness for Spectralon® at 450 nm.

The crucial assumptions made for ICAM in chapter II is that the sample is in an isotropic and homogeneous light field. In practice these conditions can not be exactly satisfied due to the energy loss by the absorption of the sample or by the leakage of radiation in the area close to the entrance or exit ports of the cavity. However, it has been shown both experimently[12,22] and by theoretical simulation[21] that the isotropy and homogeneity are sufficient in the ICAM.

4.2.3 Sample Delivery

In previous ICAMs,[22,23] the pure water was produced by a Millipore commercial purification system located outside the lab. It was delivered to the lab in quartz containers just before the experiment started. During the measurement, the water sample was siphoned out of a reservoir beneath the cavity assembly, through a Teflon® tube, and into the sample cell by a Sargent-Welch 8804 vacuum pump (5-10 psi). To minimize sample handling and to eliminate the possible contamination due to vacuum pump, a new sample delivery system together with a new Millipore water purification system was installed in the lab, as shown in Fig. IV-6.
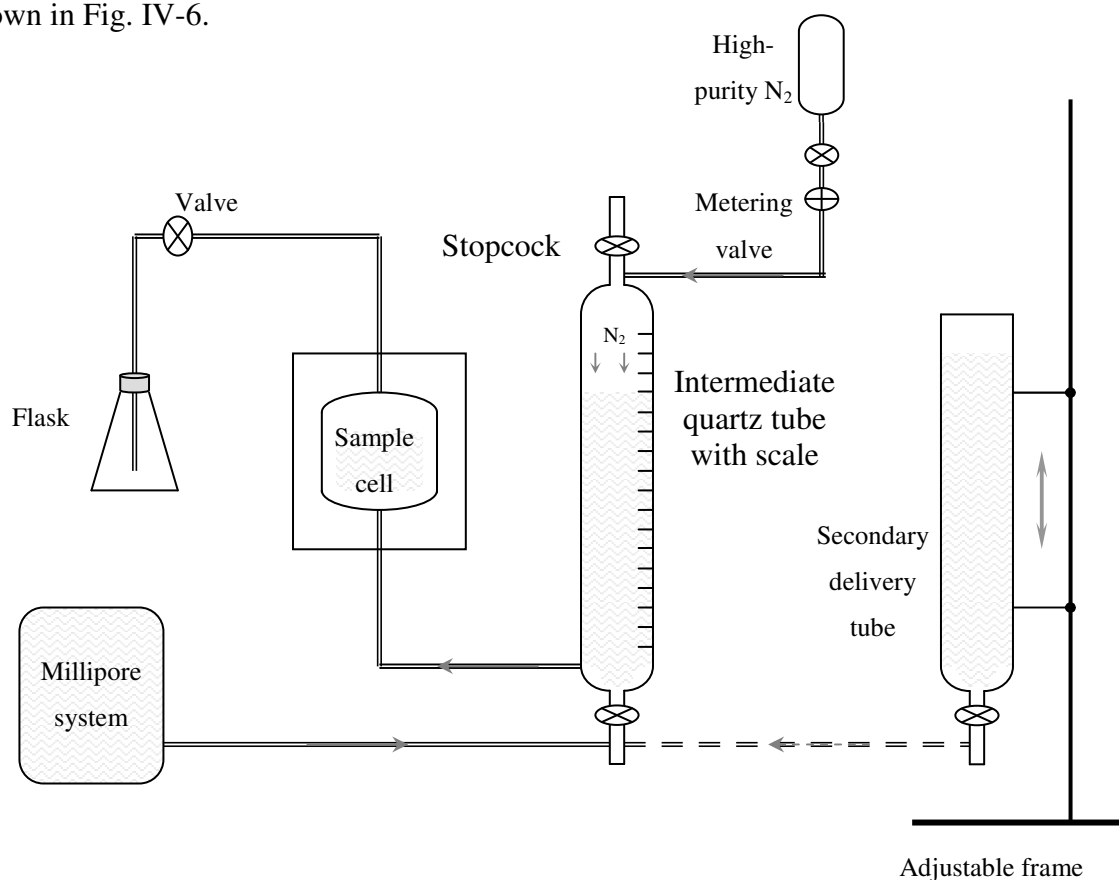
Figure IV-6. Block diagram of sample delivery system.

From the Millipore purification system, the fresh water sample flows through Teflon tube into an intermediate quartz tube. This Chemical Glass HSQ—300 quartz tube is 1000 mm long, 40 mm O.D., and 36 mm I.D.; it tapers into quartz capillary tubing at each end and into a quartz stopcock. Each stopcock consists of glass barrel, PTFE plug and FETFE O-ring. Along the quartz tube, a soft ruler with the minimum scale division of 1 mm is attached. It is used to measure the water level inside the tube; the latter can be converted into the volume of the water in the sample cell. With the help of high purity nitrogen gas, the water in the imtermediate tube is pushed into the sample cell, through a 7mm O.D., 5 mm I.D. HSQ—300 quartz tube. The flow rate of nitrogen gas is controlled by the combination of a Swagelok® metering valve and a ball valve. During measurement, the entire sample delivery system is shield from external light by aluminum foil and black curtain. The sample being measured is always sealed by high purity nitrogen gas to minimize oxygen contamination.[18,25] There is a secondary glass delivery tube mounted on a frame whose height can be adjusted. Lifting the frame allows calibration dye solutions or an acid cleaning solution in this tube to flow into the intermediate quartz tube. The secondary delivery glass tube is 1000 mm long, 40 mm O.D., 36 mm I.D., and has a glass stopcock at the bottom.

4.2.4 Detector System
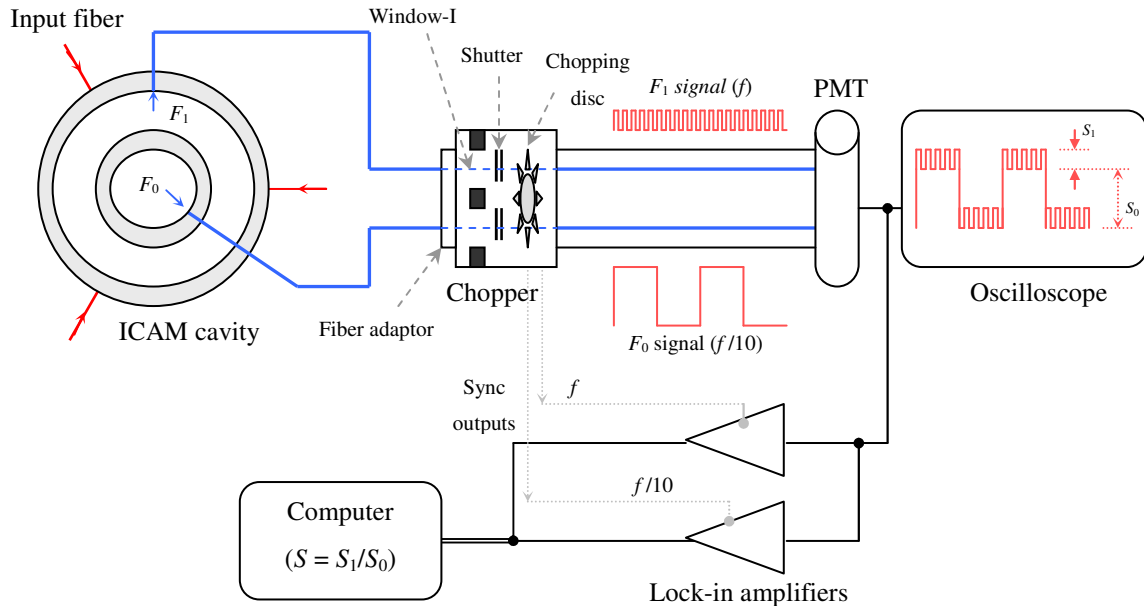
Figure IV-7. Block diagram of ICAM detector system and signal flow.

As shown in Fig. IV-7, the irradiances F_1 and F_0 are sampled through optical fibers, chopped by a two-channel light chopper with frequency f and $f/10$, respectively, and detected by a PMT. The PMT converts the combination of chopped F_1 and F_0 light into a voltage signal $S_{mix} = S_1 + S_0$ (S_1, S_0 are defined in Chapter II.). This approximately square wave signal S_{mix} provides the input to the two lock-in amplifiers. The two lock-in amplifiers extract the amplitudes of the two components S_1 and S_0 which are modulated at frequencies f and $f/10$, respectively. Finally S_1 and S_0 are sent to the computer to calculate the ICAM signal $S \equiv S_1/ S_0$.

The output fiber assembly consists of an aluminum fiber adaptor coated by black paint, and two 590 mm long, 0.37 NA TECS^{TM} coated silica/silica multimode fibers with 1.5 mm core

diameter and 2.0 mm cladding diameter. Each fiber is shielded in furcation tubing (protective cable) and both ends are carefully polished. The fiber adaptor positions the output ends of the two fibers close to the corresponding channels (windows) inside the chopper.

The light Chopper is a customized compact EG&G 197 Precision Light chopper.[37] It contains all the control circuit needed to keep the chopping disc synchronized to its internal precision oscillator or to an external trigger. The chopper has two windows equipped with manual shutters. Closing the shutter will block the light through the corresponding window. The shutters are particularly useful to check for crosstalk between the two channels. The chopping disc is made by sticking a 12 μm blade to the back disc. The blade has 30 outer apertures and 3 inner apertures. Each set of apertures chops the light from the corresponding window. The light through the window-I is proportional to irradiance F_1, similarly the light through the window-II is proportional to irradiance F_0. The outer apertures cover the frequency range 150-3000 Hz and the inner apertures cover the frequency range 15-300 Hz. Once the chopping frequency is set to a value f using a four digit pushbutton selector switch in the chopper, the light through the window-I will be chopped at frequency f, and the light through window-II is at frequency $f/10$. For each chopped signal, the amplitude is proportional to the corresponding irradiance. The chopper has two synchronous outputs which generate a 10 V nominal peak to peak square wave at the outer 30 aperture blade chopping frequency f, and at the inner 3 aperture blade chopping frequency $f/10$. They are used as reference frequencies by the lock-in amplifiers to extract the S_1 and S_0 signals from S_{mix}. The chopper is powered by an HP 6235A triple output

power supply. This extremely compact chopper together with a single photomultiplier tube reduces signal fluctuations due to random disturbances, and therefore increases the signal-to-noise ratio.

The PMT is Burle 4840 photomultiplier tube surrounded by a magnetic shield wrapped in electrical tape. The entire PTM housing is attached to the back of the light chopper by an aluminum mount. A customized power supply provides −1100V to the PMT and the output current signal is converted to a voltage signal S_{mix} by a grounded 4.6 MΩ resistor.

The lock-in amplifiers are used to extract the outer cavity signal S_1 at reference frequency f and the inner cavity signal S_0 at reference frequency $f/10$ from the PMT output signal $S_{mix,}$ and send them to the computer for data analysis. The amplifier detecting S_1 is a Stanford Research System SR 830 DSP,[38] and the amplifier detecting S_0 is an EG&G 5210.[39] Both amplifiers are controlled by the computer via the GPIB (IEEE 488) interface.

The oscilloscope is a Tektronix 210 digital real-time oscilloscope. It is used to check the PMT output voltage signal S_{mix}.

4.2.5 Data Acquisition

A Macintosh Quadra 840AV equipped with a National Instruments IEEE-488 controller provides the platform from which the ICAM is operated and controlled. The controller is connected with the GPIB (IEEE 488) interfaces of the monochromator and the lock-in amplifiers. The core of this computer platform consists of a group of LabVIEW programs which are used for instrument control, data acquisition, data display, and data analysis. Fig IV-8. shows the front panel of the main program (called VI, initials of the virture

instrument), ICAM-MAIN.vi. The other programs are sub-routines (sub-Vis) of the main program.
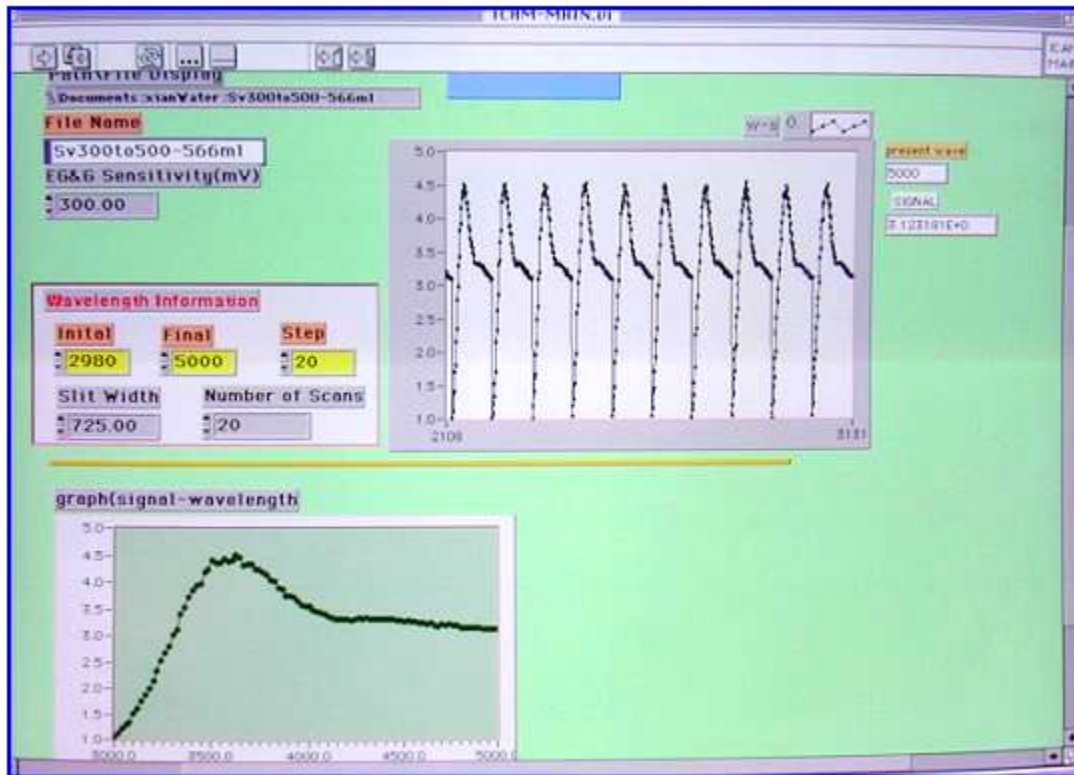
Figure IV-8. Front panel of ICAM-MAIN.vi in measurement process.

In the front panel, we can set the following control parameters: the data file name and path, the starting and ending positions with the interval (step) of the wavelength scan, the width of the monochromator slits, and the number of data points to average at each wavelength. As the ICAM-MAIN.vi starts running, it commands the monochromator to adjust the slit width and the intial wavelength; it controls the two lock-in amplifiers and reads the values of the voltage signals S_1 and S_0 extracted from S_{mix}. Once the wavelength and signal values

has been collected and processed (including averaging and calculating $S \equiv S_1 / S_0$), the computer writes the data to a file in text format. The program then moves to the next wavelength and the process is repeated until the final wavelength is reached. During the measurement, the front panel shows a graph of the real-time data for the ICAM signal S versus wavelength. If the experiment is run repeatedly, all the data are accummulated and plotted on the front panel.

4.3 Preliminary Tests

4.3.1 UV Measurement

The previously developed ICAM has been modified to extend the measurement capability into the UV. To check the performance after modification, a Newport 840C power meter with an 818-UV detector was used to measure the power from the exit slit of the Digikrom 240 monochromator and from the output end of one of the six input fibers. The 150 W Xenon arc lamp system was used with a 600 μm wide monochromator slit. Figure IV-9. shows the measured power from the exit slit of the monochromator when different monochromator gratings were used. Clearly, for absorption measurements in the UV, grating #2 must be used. Figure IV-10. shows the power from the output end of a single input fiber when using grating #2. Figure IV-11 shows the improvements 1) after optimizing the beam entering the monochromator (including adjusting the image of the arc on the entrance slit and the distance between the arc lamp and the slit) and then, 2) after optimizing the beam coming out of the exit slit (adjusting the position of the aluminum ferrule, which shields the input fibers, in relation to the exit slit).

4.3.2 Signal Test

The Tektronix 210 digital oscilloscope was used to examine the PMT output signal S_{mix} and to check the chopping and detecting process. In Fig. IV-12 (a), (b), and (c), a few examples taken from the oscilloscope show the chopped signal at several wavelengths and with two different slit widths.
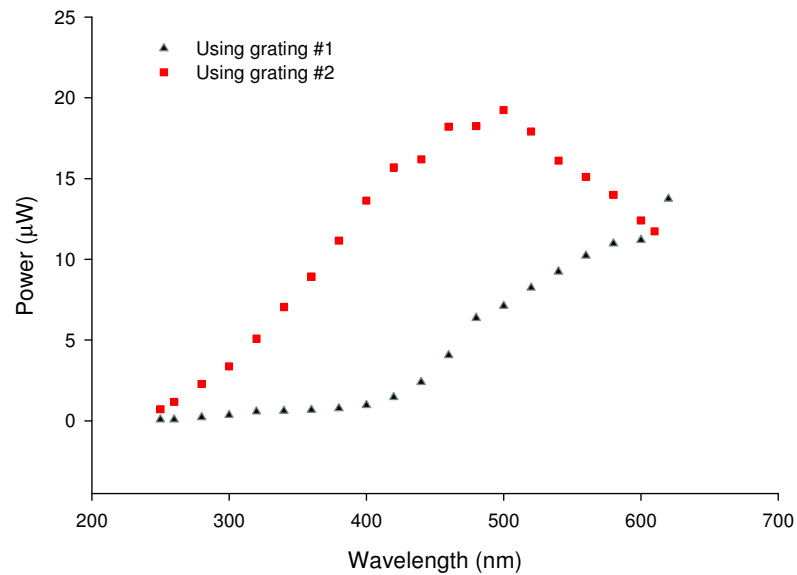
Figure IV-9. The power measured from exit slit of monochromator with grating #1 and #2, respectively (monochromator slit width = 600μm).
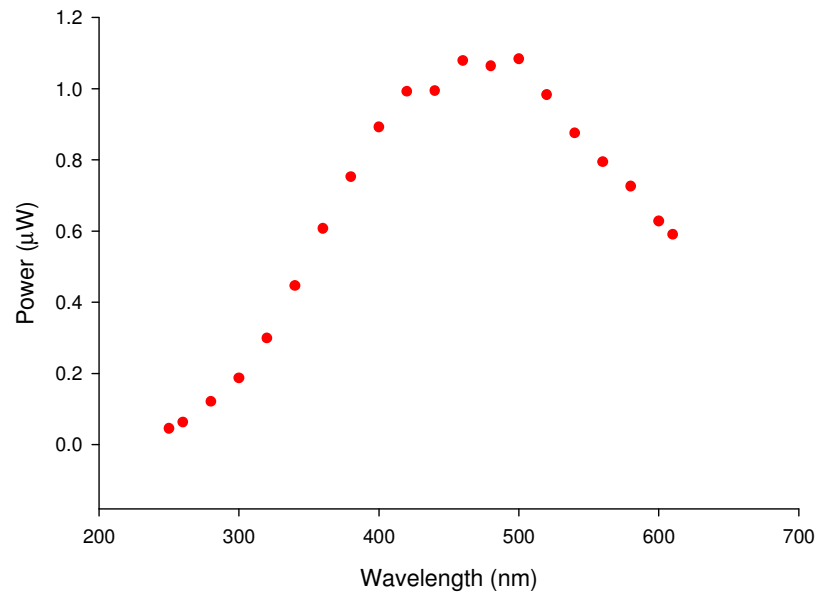
Figure IV-10. The power measured from the output end of a single input

fiber with grating #2 (monochromator slit width = 600μm).
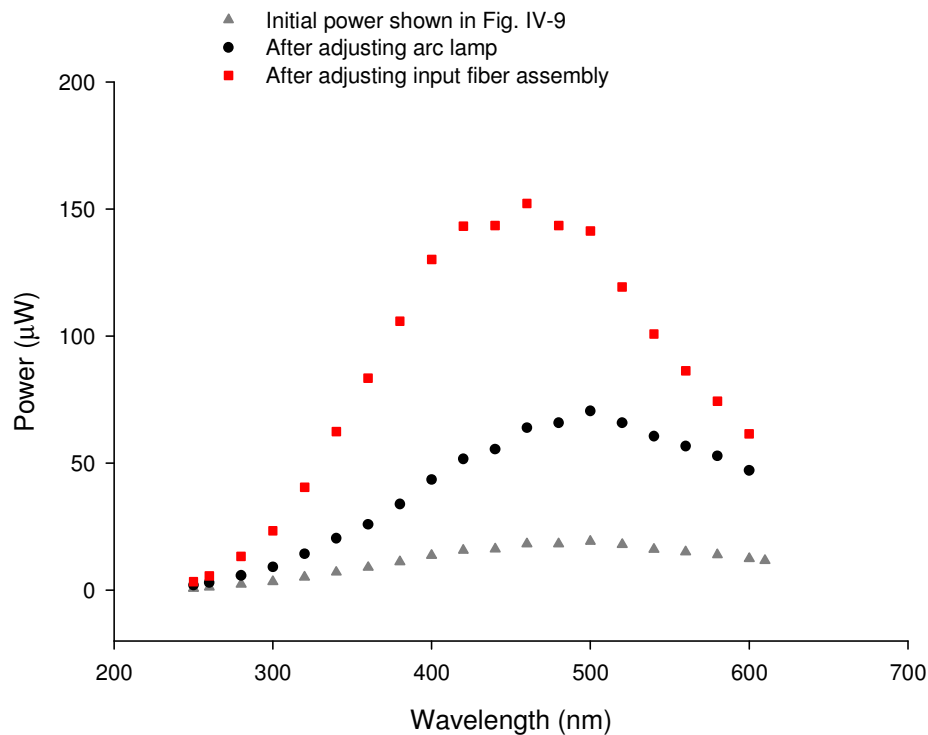
Figure IV-11. The power measured from the exit slit of monochromator at the beginning without any adjustment as shown in Fig. IV-9., then after adjusting the beam from the arc lamp, finally after adjusting the position of aluminum ferrule of the input fiber assembly (monochromator slit width = 600μm).

4.3.3 Sensitivity, Stability, and Repeatability

In the previous implementation of ICAM,[22,23] the sensitivity, stability, and repeatability tests were only made at two individual wavelengths, 500 nm and 420 nm. For the new ICAM VERSION-I, a wide range, typically 300-500 nm, has been checked to ensure the sufficiency of those tests.
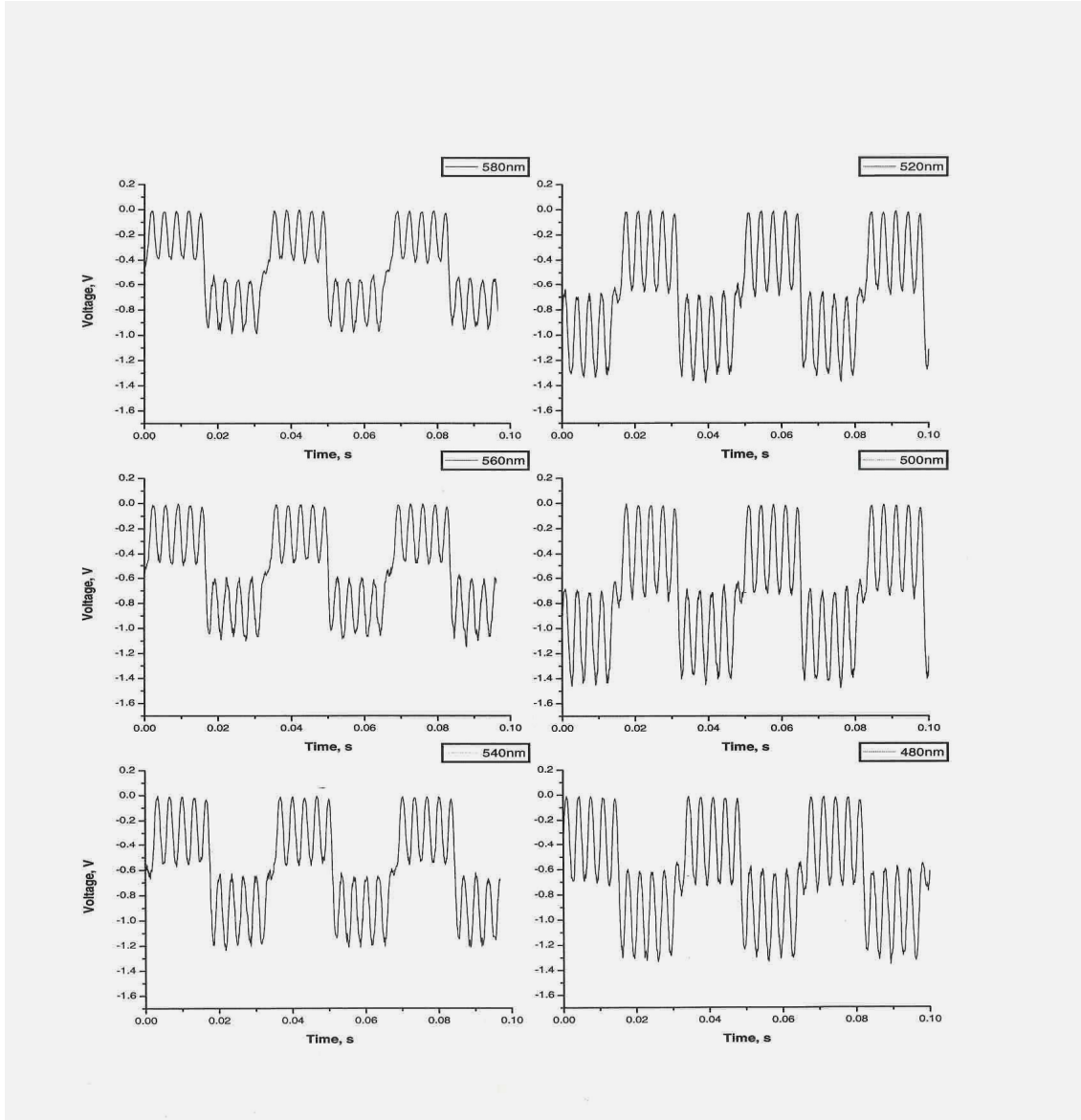
Figure IV-12 (a). The PMT output signal S_{mix} displayed on oscilloscope at several wavelengths. (monochromator slit width = 300μm).
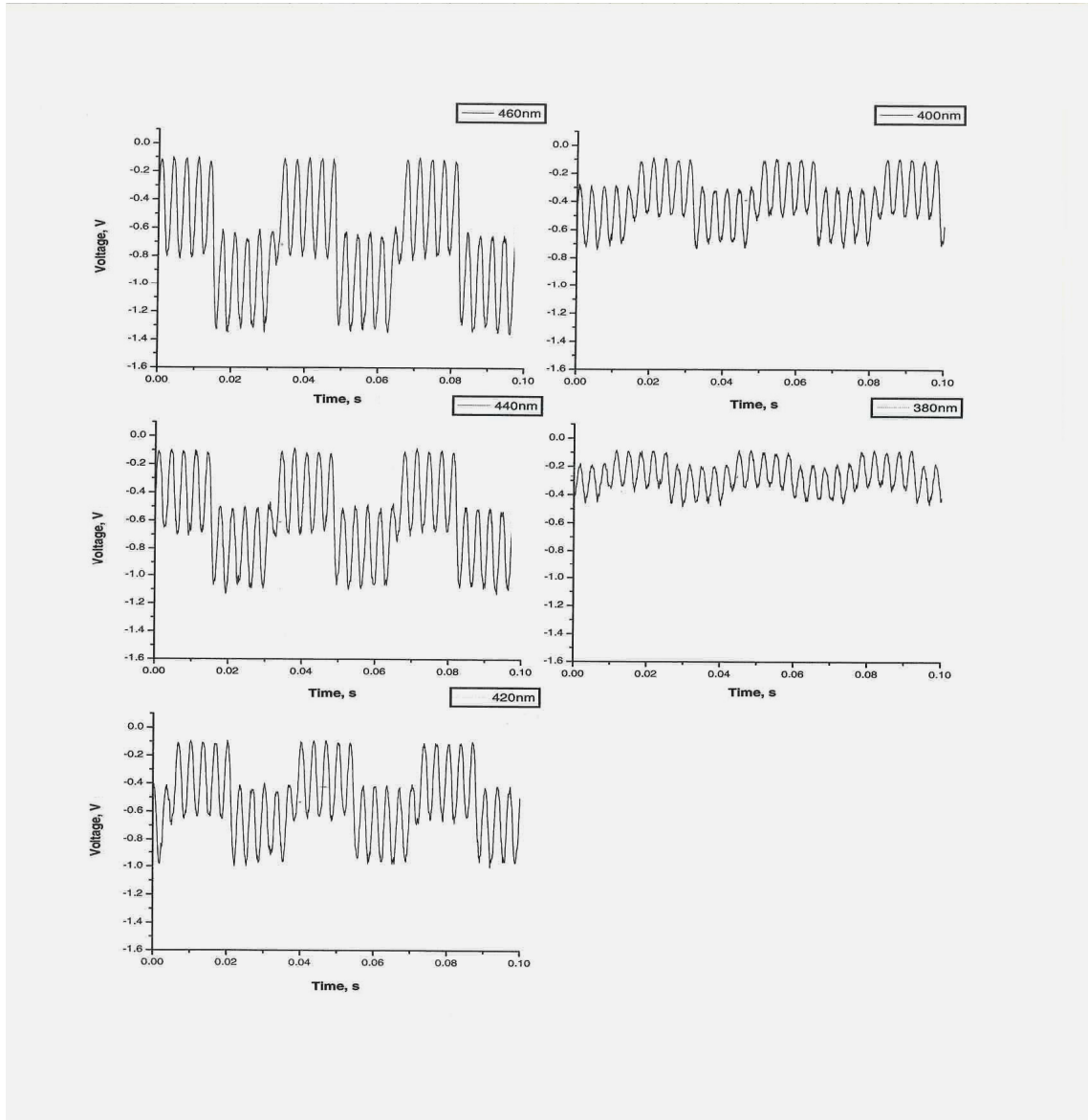
Figure IV-12 (b). Continued.
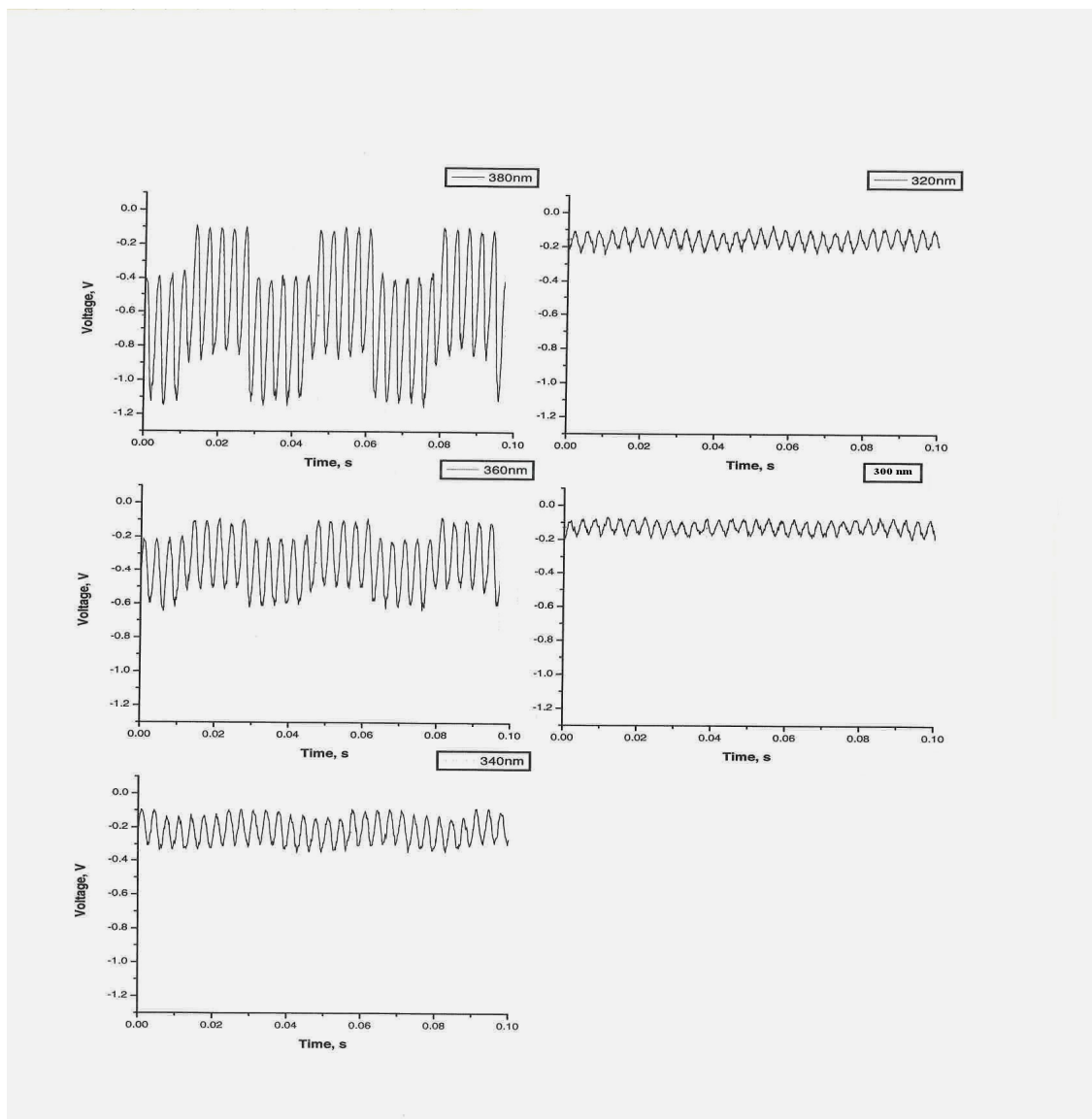
Figure IV-12 (c). Continued.

Sensitivity was examined by alternately measuring the ICAM signal with the sample cell empty (S_E) and then filled with pure water (S_F), as shown in Figure IV-13. A 150 W Xenon arc lamp was used with a monochromator slit width = 750 μm. For either S_E or S_F, the uncertainties (in percent error) for most of the wavelengths (101 data points at 2 nm intervals) are less than 1%. For example, the uncertainties of S_E are less than 1% at 82 points, 1% - 1.5% at 9 points, 1.5% - 2% at 7 points, and 2% - 3% at only 3 points. These numbers of points for such corresponding uncertainties of S_F are 80, 8, 11, and 2. Higher uncertainties occur mainly in the region below 350 nm.
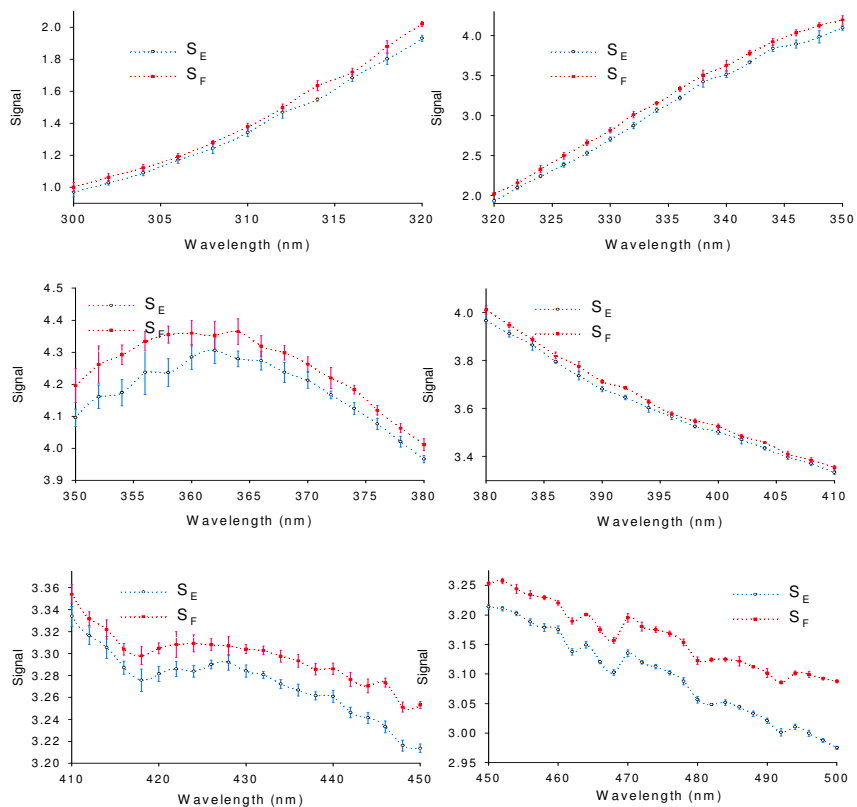
Figure IV-13. ICAM sensitivity test by measuring empty cavity signal S_E and full cavity signal S_F alternately in the wavelength range of 300-500 nm.

Stability was checked by recording the cavity-empty signal S_E at given time intervals, typically every one hour, over a period of at least 6-8 hours, as shown in Fig. IV-14.
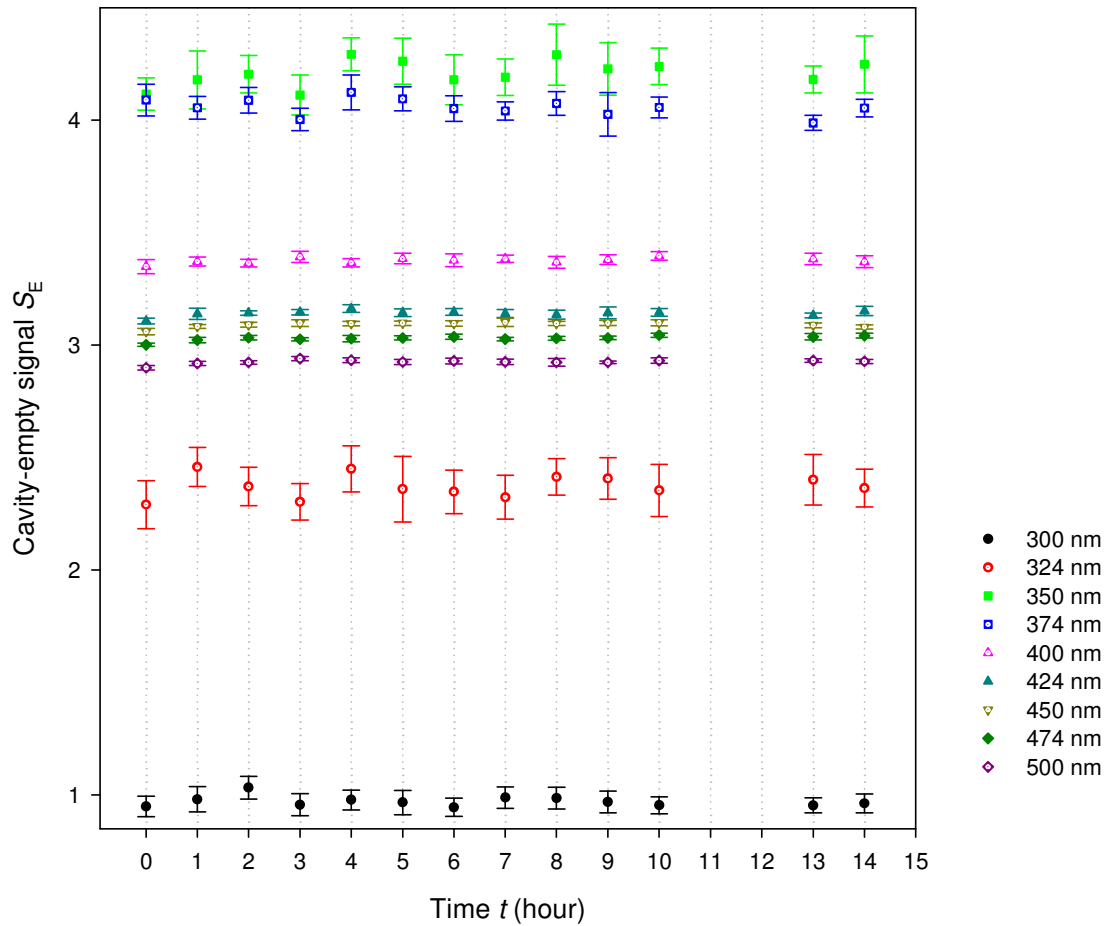
Figure IV-14. ICAM stability test by recoding the cavity-empty signal S_E at 1 hour intervals over 14 hours, here $t = 0$ is the time right after turning on all the equipment.

Repeatability was determined by recording a single measurement of cavity-empty signal S_E and cavity-full signal S_F on three successive days, then calculating the signal (S_E, S_F)

difference between successive days. The results are shown in Fig. IV-15. For both S_E and S_F, the differences were on the order of ~ 1% compared to the average of S_E (or S_F) on successive days.

These experimental results show the sensitivity of the ICAM VERSION-I to the changing absorption between the empty cell and the cell filled with pure water, the stability of the cavity-empty signal over several hours of operation, and the repeatabilities of both the cavity-empty signal and cavity-full signal on successive days.

4.4 Absorption Measurement

Pure water absorption measurements begin by measuring cavity-empty signals S_E, which act as baseline for the ICAM, followed by measuring cavity-full signals S_F at 2 nm intervals over the entire wavelength region. Before the experiment starts, the sample cell and the entire sample delivery system are purged with high purity nitrogen gas. Typically, both S_E and S_F are repeatedly measured 5-7 times; this permits analysis of the repetitive signals to determine the stability and repeatability of the signal, and to improve signal to noise ratio by averaging the results. The pure water sample is changed every time S_F is measured to ensure that a fresh sample is being examined, and the samples are always sealed by high purity nitrogen gas (99.998%).
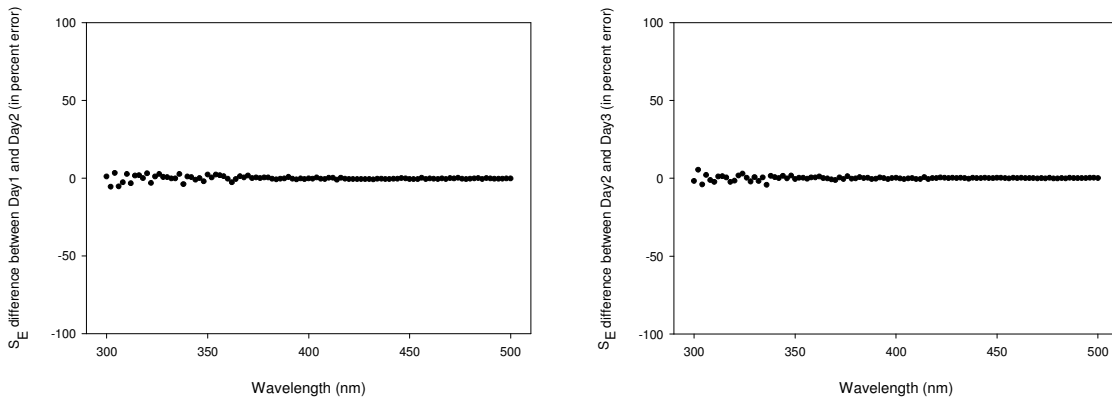
(a) Cavity-empty signal
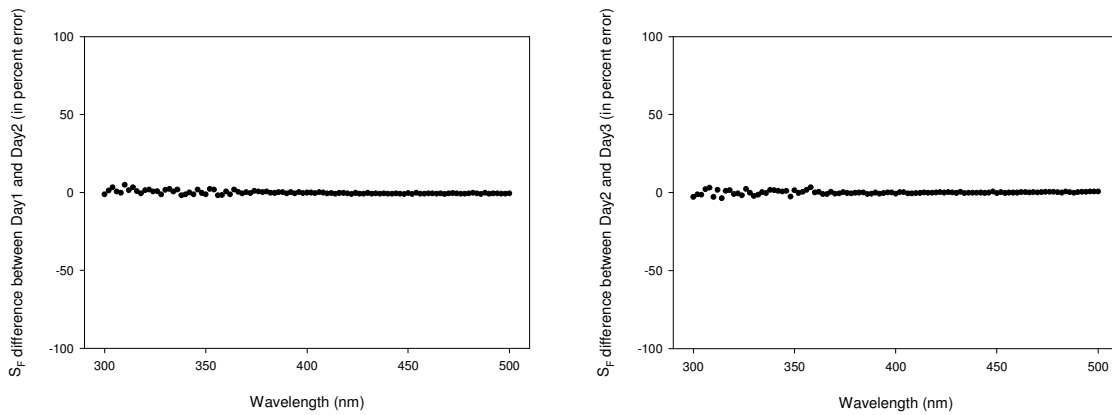
(b) Cavity-full signal

Figure IV-15. ICAM repeatability test by recording cavity-empty signal S_E and cavity-full signal S_F on successive three days, then finding the signal difference, S_F - S_E , on two successive days and comparing this to their average value (percent error).
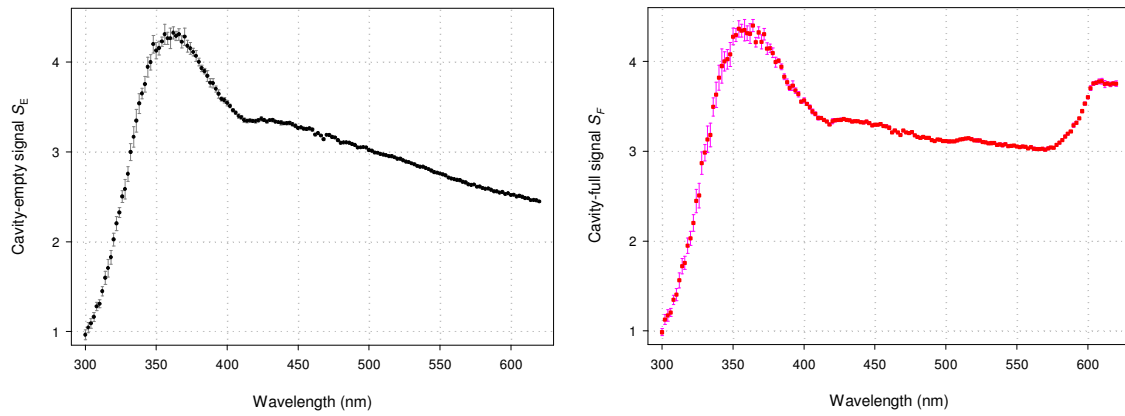
Figure IV-16. Single measurement of ICAM cavity-empty signal (left) and cavity-full signal (right) with error bars.
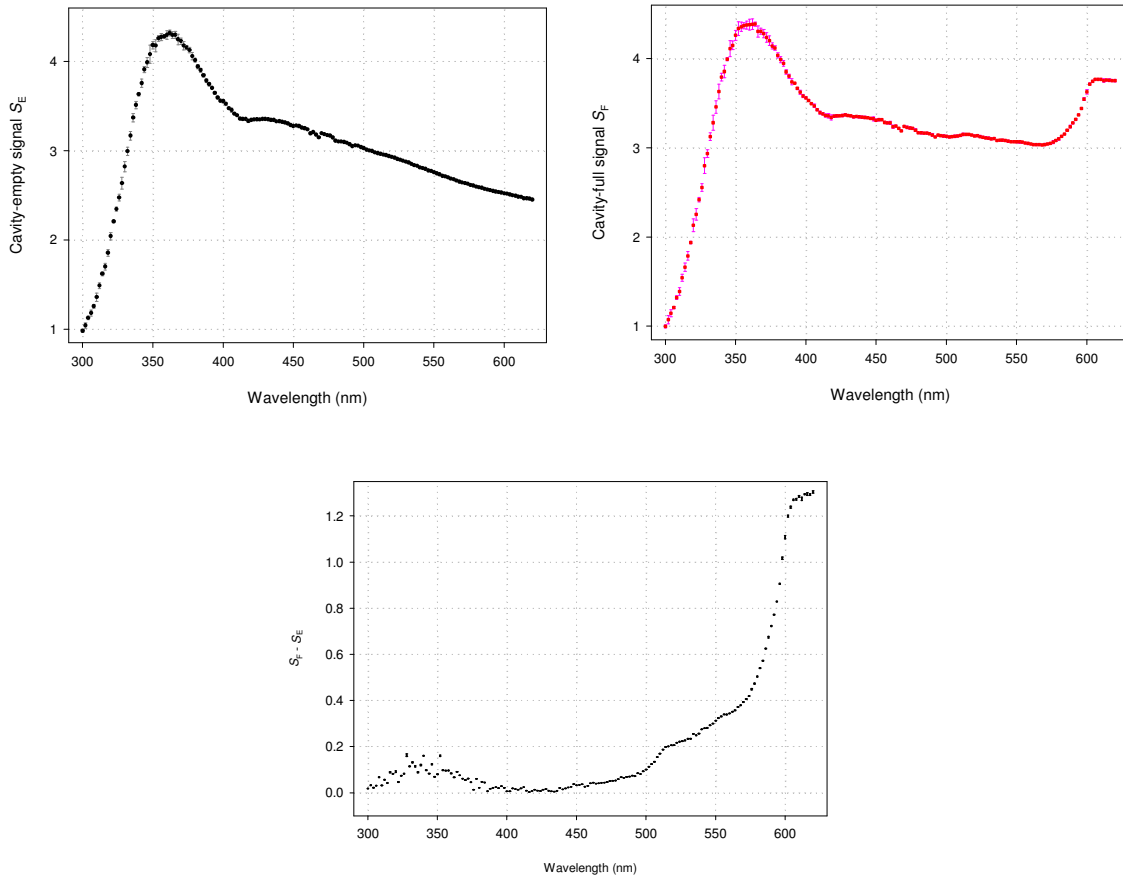
Figure IV-17. Average of 5 repetitions of ICAM cavity-empty signal (top left), average of 4 repetitions of cavity-full signal (top right), and the difference between them (bottom).

Fig. IV-16 shows a single measurement of S_E and S_F with error bars. Fig. IV-17 then shows the average of 5 S_E and of 6 S_F measurements with statistical uncertainties, followed by the difference between them, i.e. S_F - S_E. As indicated by these graphs, the uncertainty of a single measurement in Fig. IV-16 is consistent with the standard deviation when

repetitive measurements are averaged together in Fig. IV-17. During the absorption measurements and both calibration procedures described in the following sections, the temperature of the pure water from the purification system was stable at 25 °C (±1 °C), with 18.2 MΩ resistivity and TOC 4 ppb (±2 ppb).

4.5 Calibration

The offset calibration is always performed before the normalization calibration because the former only involves pure water sample but the latter involves dye solutions which can introduce contamination to the sample delivery system.

4.5.1 Offset Calibration

As described in Chapter II, the offset calibration is based on the function $S(V)$ which is the ICAM signal S versus sample volume V obtained by measuing a set of pure water samples with different volumes. The Calibration starts with a cavity-empty signal measurement (defined as $S(0)$ identical to S_E), followed by measuring 10-15 pure water samples in a sequence of equally increasing volume, until the last sample, $S(566)$ which is identical to cavity-full signal S_F (566 is the total capacity of the sample volume in millilitre). Examples of $S(V)$ at several wavelengths are plotted in Fig. IV-18. During the entire measurement process, each sample is sealed by high purity nitrogen gas.
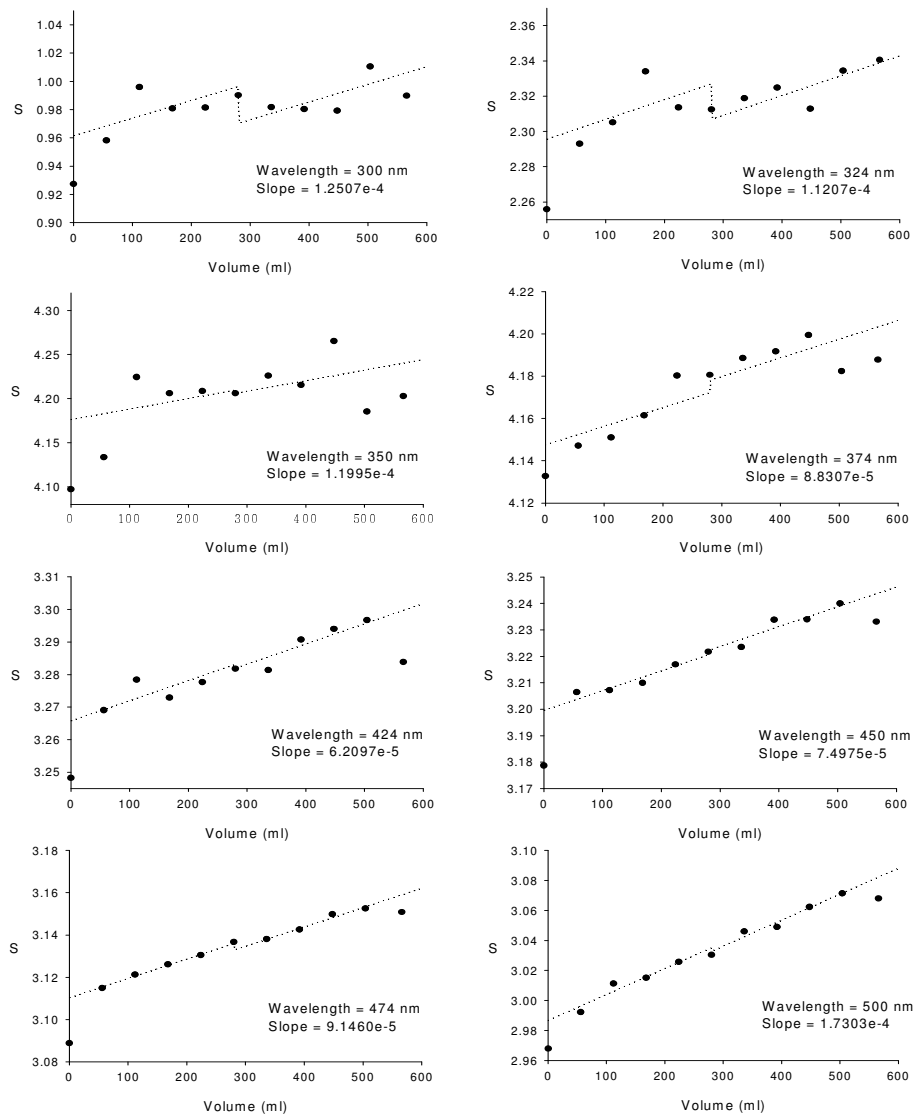
Figure IV-18. The signal *S* as a function of the volume *V* at eight wavelengths. Also shown is the linear least-square fitting line discussed in Chapter II.

4.5.2 Normalization Calibration

As described in Chapter II, the normalization calibration is based on the function $\alpha(S)$ which is the absorption coefficient α of the dye versus the ICAM signal S. It is measured by first measuring a pure water sample, followed by measuing 8-10 dye solutions in a sequence of increasing concentrations.

A "master" dye solution was prepared by dissolving the dye powder (on the order of a milligram) in pure water, then filtering the dye solution through Gelman Supor®-200 47 mm diameter, 0.2 μm membrane filters. The absorption (A) of the "master" dye solution was measured at 1 nm intervals over the wavelength region from 200 nm to 700 nm in a Varian Cary100 spectrophotometer in the Chemistry department. The absorption due to the dye, A_{dye} was obtained by placing two identical Fisher standard cells (3 ml, 10 mm lightpath, with Suprasil quartz windows) filled with "master" dye solution and pure water, respectively, into two equally separated beams of the spectrophotometer, then measuring the absorption due to the dye solution $A_{solution}$, and the absorption due to pure water, A_{pure} $_{water}$. Finally the dye absorption $A_{dye} \equiv A_{solution} - A_{pure\ water}$ is calculated and saved as a function of wavelength. This absorption A_{dye} is converted to absorption coefficient α_{dye} (as defined in Chapter II) in units of m^{-1} by using the following equation:

$$\alpha = \frac{\ln 10}{L} \times A, \tag{4.1}$$

which is simply derived from the definition of absorption used in the Chemistry lab,

$$A \equiv \log_{10}(I_o / I), \tag{4.2}$$

where L is the light path of a standard quartz cell, I_o is the input source intensity, and I is the intensity transmitted through the standard quartz cell.

Three water soluble dyes have been used for the normalization calibration: Irgalan Black (black powder), Alcian Blue (blue powder), and Nigrosin (black powder). Three "master" dye solutions made by using one or two of these three dyes were measured, their absorption spectra are plotted in Fig. IV-19. The Alcian Blue increases the absorption of the dye solution in the red region, as shown in Fig. IV-19. However, when performing calibration measurements by using dye samples diluted from the "master" dye solution made by the combination of Irgalan Black and Alcian Blue, we constantly observed some negative values of $S_{dye} \equiv S_{solution}$ - $S_{pure\ water}$ in the UV region, specifically below 350 nm. The explanation is that this unusual "negative absorption" is due to fluorescence of the Alcian Blue dye.[40] Consequently, none of the normalization calibration results presented in the rest of this dissertation used the Alcian Blue dye. Compared to Nigrosin dye, the Irgalan Black has relatively flat absorption spectrum, therefore it is ideal for normalization calibration purpose.

After the "master" dye was prepared and measured, it was then volumetrically diluted to produce 10 samples, designated Cal#1 through Cal#10 (Cal#0 for pure water sample), with corresponding absorption coefficients ranging from approximately 0.015 m^{-1} to 0.15 m^{-1} at 417 nm, where the pure water was found to have the minimum absorption.[10,22,23] For each sample the absorption uncertainty is approximately 1% due to uncertainties in the volumetric dilution of the dye solution.

Irgalan Black master dye made by dissolving 40mg Irgalan black in 1000ml of pure water, Nigrosin master dye made by dissolving 40mg Nigrosin dye in 1000ml of pure water, and Irgalan Black plus Alcian Blue master dye made by dissolving 70mg Irgalan Black and 30 mg Alcian Blue in 2500ml of pure water.
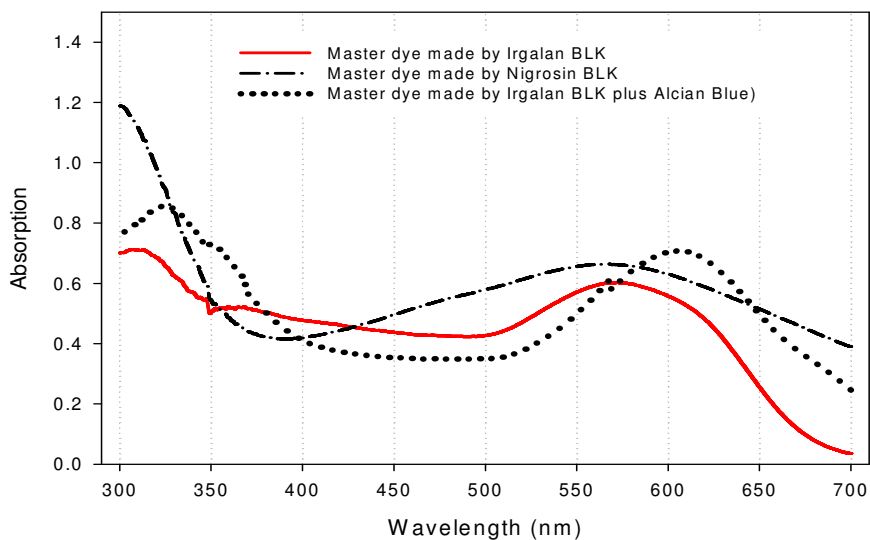
Figure IV-19. Absorptions of three "master" dye solutions measured by Cary100 spectrophotometer.

All the samples, Cal#0 through Cal#10, were successively placed in the ICAM VERSION-I, in a sequence of increasing dye concentration, and for each sample the signal was measured as a function of wavelentgh. At each wavelength, the values of α_{dye} calculated from the absorption coefficient of the "master" dye divided by the dilution factors for the 10 solutions), were plotted as a function of $S_{dye} \equiv S_{solution} - S_{pure\,water}$, where $S_{solution}$ is the signal for dye solution and the $S_{pure\,water}$ is the signal for pure water. Fig. IV-20 shows examples of $\alpha_{dye}(S_{dye})$ at several wavelengths using a "master" dye made by Irgalan Black, and Fig. IV-21 shows the final result for the calibration constant C_1'' obtained by linearly fitting $\alpha_{dye}(S_{dye})$ data and then finding the slope (discussed in Chapter II).
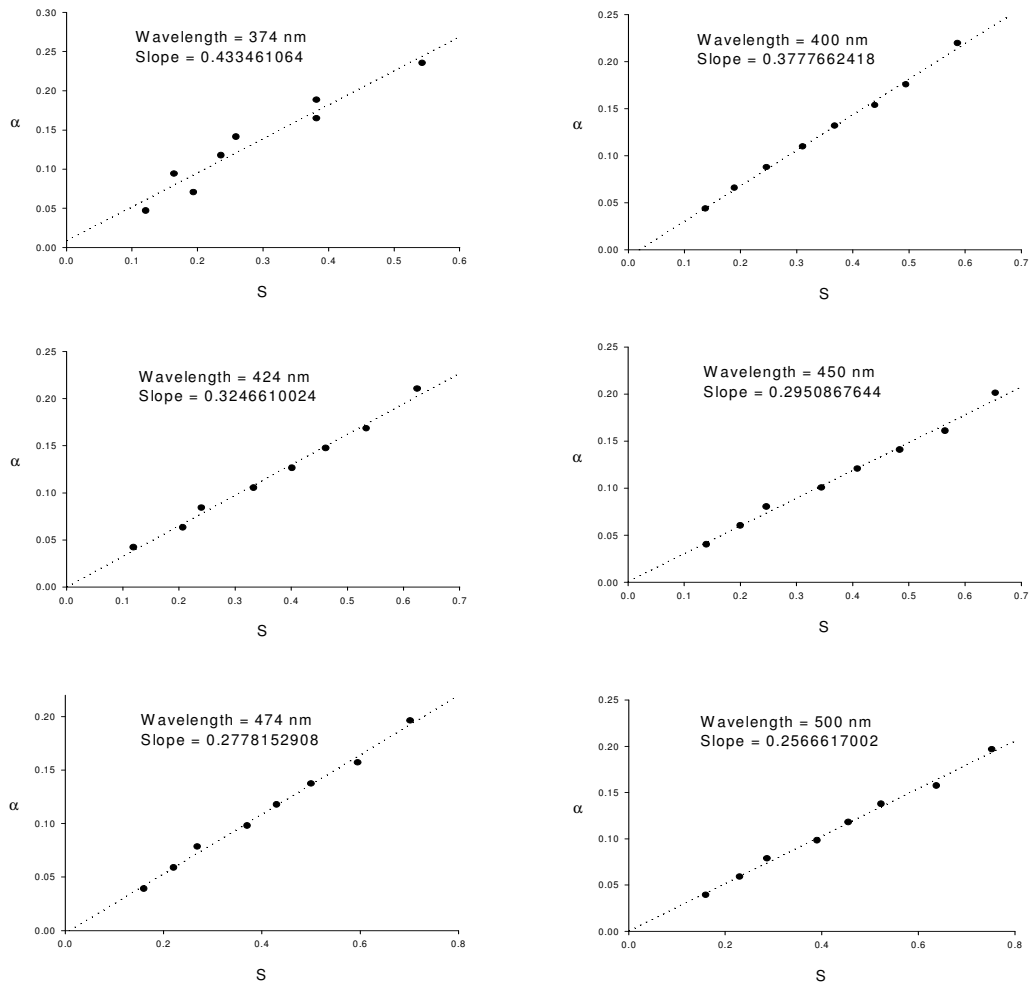
Figure IV-20. The absorption coefficient α as a function of signal S at six wavelengths. Also shown is the linear least-square fitting lines discussed in Chapter II.
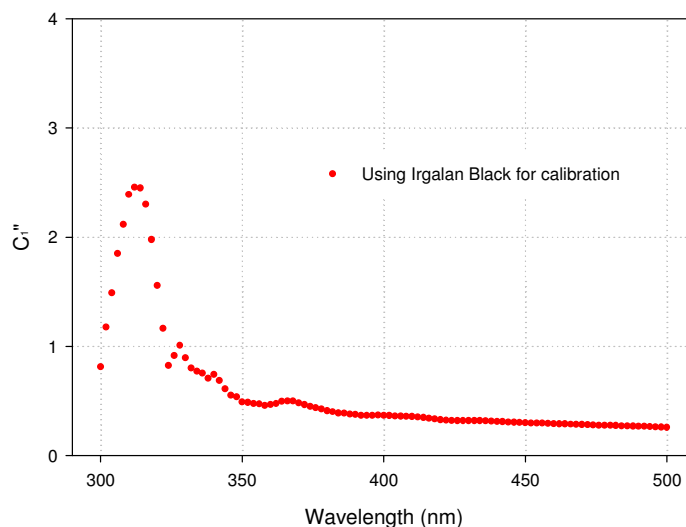
Figure IV-21. Normalization calibration constant C_1'' as a function of wavelength.

4.6 Results

The absorption coefficients of pure water in the region from 300 nm to 500 nm observed with the ICAM VERSION-I showed unrealistic and inconsistent values of absorption in this spectrum region.[41,42] The problem is a consequence of the absorption and degradation of Spectralon[®].

4.7 Spectralon[®] Absorption and Degradation

As indicated in both Table IV-1 and Table IV-2, the typical reflectance of Spectralon® decreases from 99.1% at 400 nm to 98.4% at 300 nm. One key feature of the ICAM is its capability to measure very low values of the absorption coefficient due to the long path length that the light travels through the sample. However, this requires that the cavity wall

reflectivity is maintained at a high value. A decrease in reflectivity of ~1% more than halves the path length in weakly absorbing ocean water.[21] As a consequence, both the sensitivity of the ICAM and the signal to noise ratio are reduced.

The decreased reflectivity is mainly due to Spectralon® absorption. The "ageing" of Spectralon® is the main reason leading to degradation of the diffuse reflectance. Several conditions could lead to this "ageing" problem: radiation wavelenth; radiation exposure level and time; and storage time. Significant reductions in the reflectrance (at 400 nm) of Spectralon® samples stored in a dark, air-tight box have been reported.[47] As examples, the reflectance at 350 nm of several Spectralon® samples was shown to decrease with age: from 0.985 (1 year storage), to 0.981 (3 years), to 0.979 (4 years), to 0.968 (5 years), and to 0.926 (9 years). Similarly, a reduction was observed from 0.991(1 year) to 0.968 (9 years) at 500 nm. The reduction of reflectance in the UV was much greater than in the visible region. Furthermore, the ageing effects of Spectralon® under high-level radiation have been reported by different groups.[43-46]. Usually Spectralon® was assumed to be relatively stable under low-level radiation. But recent studies showed that low levels of exposure in the UV and visible range could induce a spectrally dependent reduction of reflectance in the UV range even after sereral hours irradiation (1% drop after 94 hours exposure to a 254 nm UV lamp).[47,48]

CHAPTER V

ICAM VERSION-II

The unrealistic and inconsistent values of absorption of pure water observed using ICAM VERSION-I indicated that even more serious modifications were required. A new material is necessary to replace the Spectralon® as the diffuse reflecting wall of the integrating cavity. Historically, the most commonly used materials for the diffuse reflector have been magnesium oxide, opal glasses, ceramic tiles, barium sulfate powder or paint, later on the Spectralon®, and Polytetrafluoroethylene (PTFE, which is better known by the trade name Teflon®) powder.[49,50] Among these reflecting material, Spectralon® and PTFE powder show the highest reflectivity (the latter has slightly higher reflectivity than the former in visible but they are the same in the UV). V.R. Weidner and J.J. Hsia reported the diffuse reflectance of pressed PTFE powder is "remarkably" high over the spectral range of 200-2500 nm and is probably higher than that of any other material at their time.[51] However, like Spectralon®, PTFE has the absorption problem in the UV. Therefore, both Spectralon® and PTFE are particularly useful for integraing cavity purpose over the spectral range of 350-1800 nm (99% or higher reflectivity), but not for the application below 350 nm.

5.1 Quartz Powder

After extensive investigation, we developed a new diffuse reflecting material in order to use the integrating cavity in the UV. The ultra-pure fused silica powder is the well known optical material with high transmission and negligible degradation problem. The pressed quartz powder (average particle size is on the order of sub-micron) shows even higher

reflectivity (99.7%) than Spectralon® in the UV and visible. This high reflectivity is due to the multiple interface between the quartz particles and surrounding media (e.g., the air). The pressed quartz powder can be used as diffuse reflector in a wide range of applications. It can dramatically improve the sensitivity of the integrating cavity absorption meter. It can be used to build other devices for spectroscopic measurements. Furthermore, its high reflectivity and negligible degradation lead to potential applications in optical coupling system (e.g., solid state laser pumped by flash lamp or laser diode).

In this work, the pressed quartz powder was used to build a new inner cavity to replace the Spectralon® inner cavity in the ICAM VERSION-I. The new instrument was named ICAM VERSION-II.

5.1.1 Preliminary Test

The reflectance of the pressed quartz powder was experimentally examined by using the ingegrating cavity technology. Fig. V-1 shows the experimental setup for measuring the reflectivity of the pressed quartz powder relative to the Spectralon®. A 532 nm laser beam was aligned to pass through the top and bottom holes on a cubic Spectralon® integrating cavity with a 8˚ angle off the vertical axis Z. The laser beam was diffusely reflected by the surface of a Spectralon® block beneath the bottom hole of the cavity. On one side of the block a portion of the Spectralon® was removed to make a cavity filled by pressed Pegasus fused silica powder. The pressed powder was flush with the surrounding Spectralon® part. The diffuse reflected light was collected by the integrating cavity, and then reached the PMT through a side hole on the cavity after undergoing multiple internal reflections. The Spectralon® block was mounted on a motor. When the motor was running at a constant

speed, the incident laser beam was reflected by the Spectralon® surface and the quartz powder surface alternately. Therefore the output voltage signal from the PMT was a modulated signal with varied peak values proportional to the reflectivity of the corresponding surface. An oscilloscope was used to measure this signal. A neutral density filter covered the top hole on the cavity to reduce the laser intensity. A Spectralon® screen
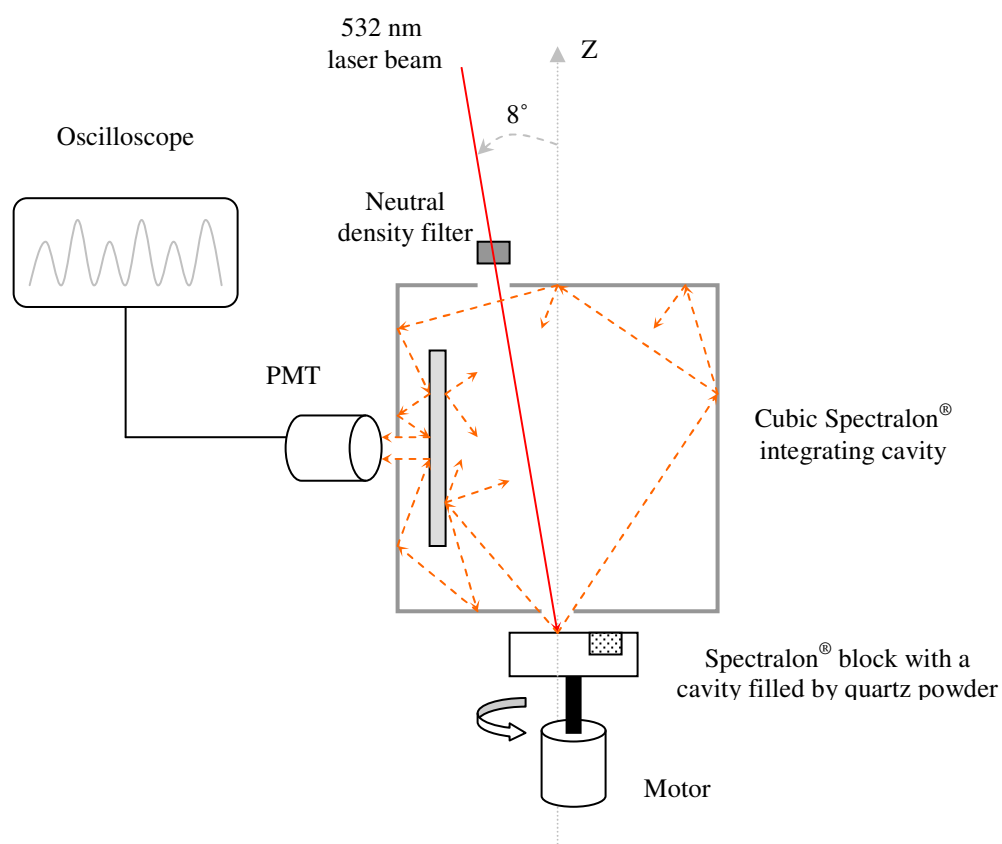
Figure V-1. Experimental setup to measure the reflectivity of quartz powder relative to Spectralon®.

was placed inside the integrating cavity to prevent the PMT from "seeing" the directly reflected light from the Spectralon® without multiple internal reflections.[51] The experimental results shown in Fig. V-2 indicates the reflectivity ratio of the pressed quartz powder to the Spectralon® is about 1.021.
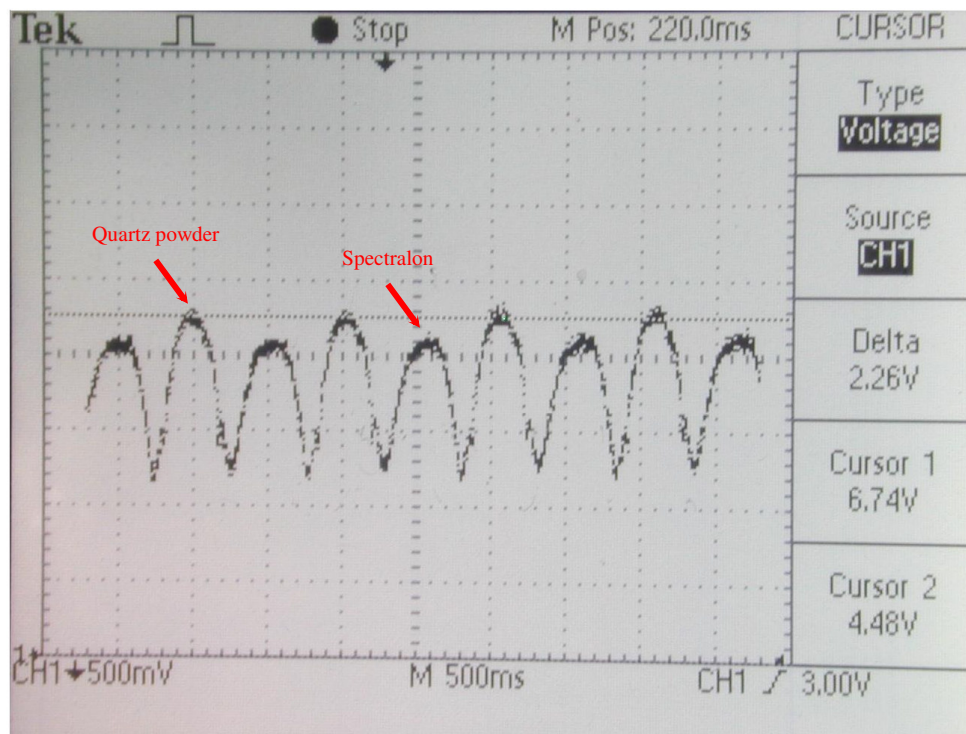
Figure V-2. Experimental result of measuring the reflectivity of pressed quartz powder relative to Spectralon® with 532 nm laser and rotational speed of 1 rev/sec.

5.2 New Integrating Cavity Assembly

5.2.1 Configuration

Figure V-3 is the corss section of the ICAM VERSION-II. Compared to the ICAM VERSION-I, the crucial change is the inner cavity part. The previous Spectralon® inner cavity was replaced by a fused silica cell. It consists of a TOSOH ED-H synthesized silica glass wall which is 152 mm long with a 96.5 mm I.D. and a 105 mm O.D.; two end caps made of TOSOH ES Ground Disc with a 101 mm diameter and a 20 mm diameter center hole; and two Suprasil 300 fused silica tubes with a 17 mm I.D. and a 20 mm O.D. Each tube is welded to one end cap. To make a strong connection the bottom cap is welded together with the cylindrical wall. A 15 mm hole is dirlled at the mid-point of the cylindrical wall for inserting the output fiber (detecting F_0). The quartz sample cell is embeded in the pressed quartz powder which fills the space between the inner cavity quartz cell and the sample cell. At both ends of the cavity, the powder is sealed by two Spectralon® plugs. A modification has been made to the quartz sample cell used in ICAM VERSION-I. An 8 mm O.D., 2 mm I.D., 2 mm thick fused silica plate is welded to the sample cell in its mid-point. This small plate is to position the F_0 detecting fiber, which is shielded by a Spectralon® tube.
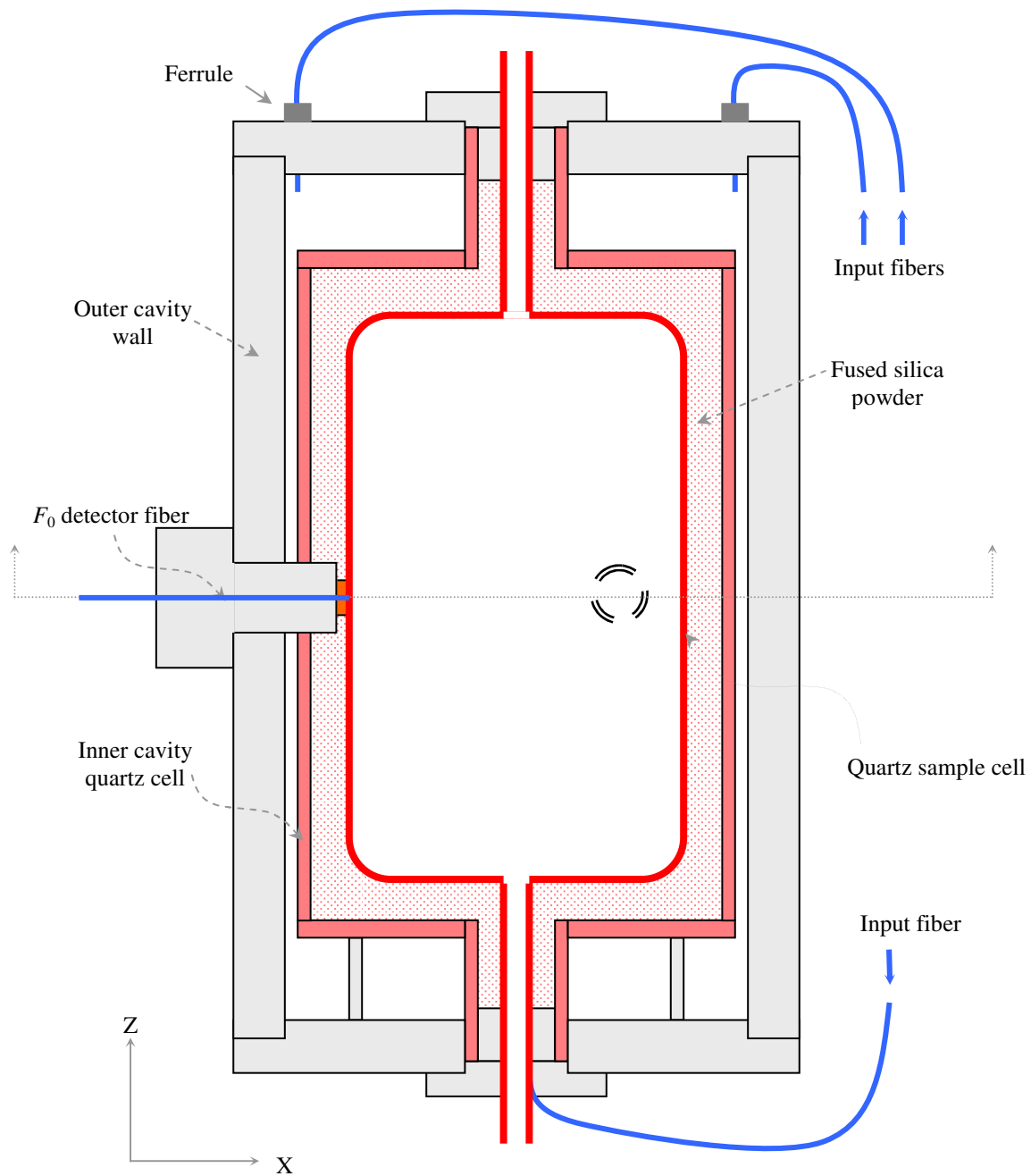
Figure V-3. Cross sections of the integrating cavity assembly perpendicular to *Y* axis in the ICAM VERSION-II.

5.2.2 Quartz Powder Handling

The Pegasus fused silica powder was fluffy as it arrived in a glass container. Before it was put into the cell, the powder was baked to remove the absorbed moisture and the other organic content. A quartz tube containing the powder was put into an oven whose temperature was controlled through a transformer. Immediately after the baking process, the baked quartz powder was filled into the cavity step by step. In each step, a small portion of quartz powder was added to the cavity using a quartz plate and pressed by a flat end quartz rod. The entire cavity assembly (including the irradiance F_0 detecting fiber shielded by the Spectralon® tube) was set up in a hood and the specific mask and eye goggles were required for safety issue. The cavity assembly was mounted on two height adjustable stages and the sample cell was fixed in the center (along Z axiz) to ensure the thickness of the pressed powder was uniform. During powder filling process, 4 of the 6 Spectralon® side wall parts were removed so that we could monitor the pressing process. A flash lamp was used to introduce the illumination light into the cavity through the inlet tube of the sample cell after the room light was turned off. With this illumination light we could locate possible bright spot which indicated a leakage due to a small portion of powder which was not pressed tightly.

5.3 Absorption Measurement

Absorption measurements started by measuring 4 cavity-empty signal S_E, followed by measuring 4 cavity-full signal S_F. The signal difference $S_F - S_E$ is plotted in Fig. V-4 together with the the signal difference $S_F - S_E$ result measured by the ICAM VERSION-I.
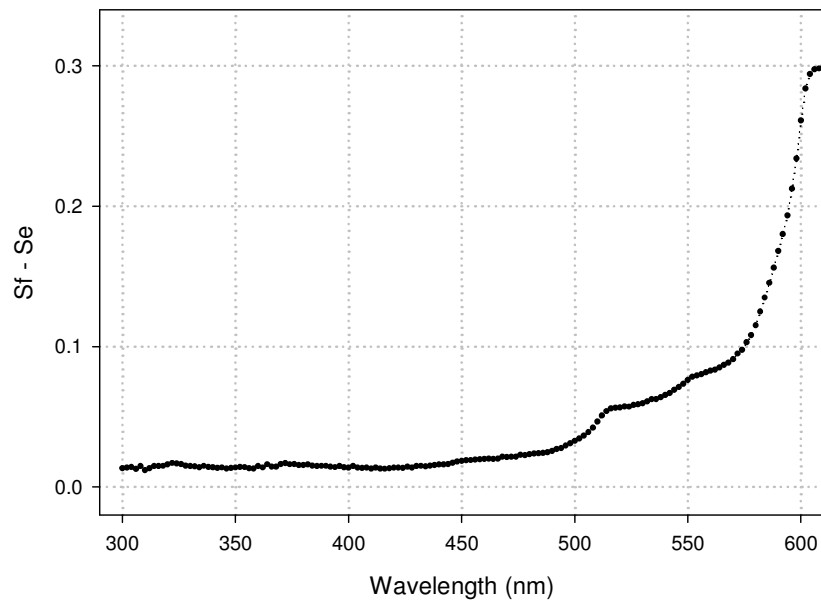
(a)

ICAM VERSION-I : S_F - S_E

ICAM VERSION-II : S_F - S_E
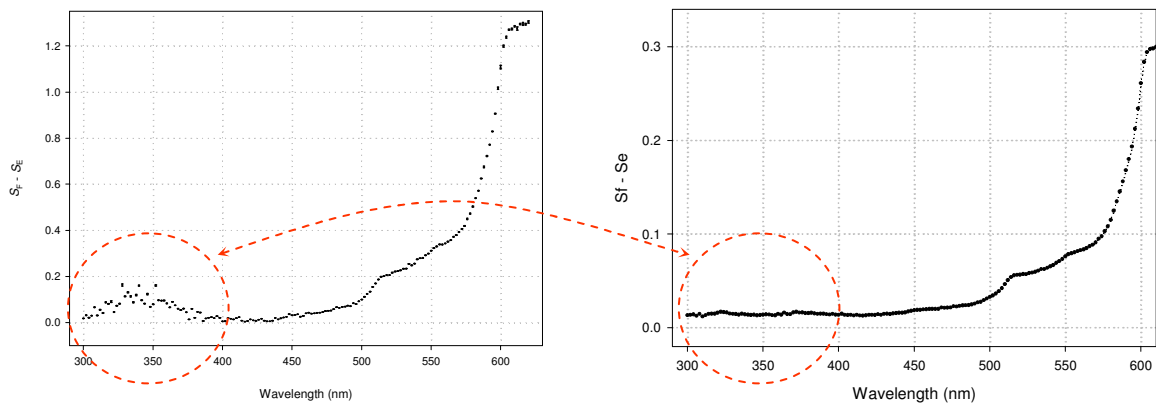
(b)

Figure V-4 (a) The difference between the average of 4 cavity-empty signals (S_E) and the average of 4 cavity-full signals (S_F) measured by ICAM VERSION-II. **(b)** Comparison between ICAM VERSION-I and VERSION-II.

The latter shows a bump formed by scattered data points in the region of 300-400 nm, while the former shows a relative flat curve in the same region.

5.4 Calibration

Calibration procedure was similar to that of ICAM VERSION-I described in Chapter IV.

5.4.1 Offset Calibration

The signal S as a function of the sample volume V at 7 wavelengths are ploted in Fig. V-5 with linear fitting results. The offset function $s(\lambda)$, which was discussed in Chapter II, is plotted in Fig. V-6 with the fitting result and the offset constant C_0".

5.4.2 Normalization Calibration

The absorption coefficient α of calibration dye (Irgalan Black) as a function of the ICAM signal S at 7 waelengths are plotted in Fig. V-7 with linear fitting results. And the normalizationg constant C_1" is plotted in Fig. V-8.
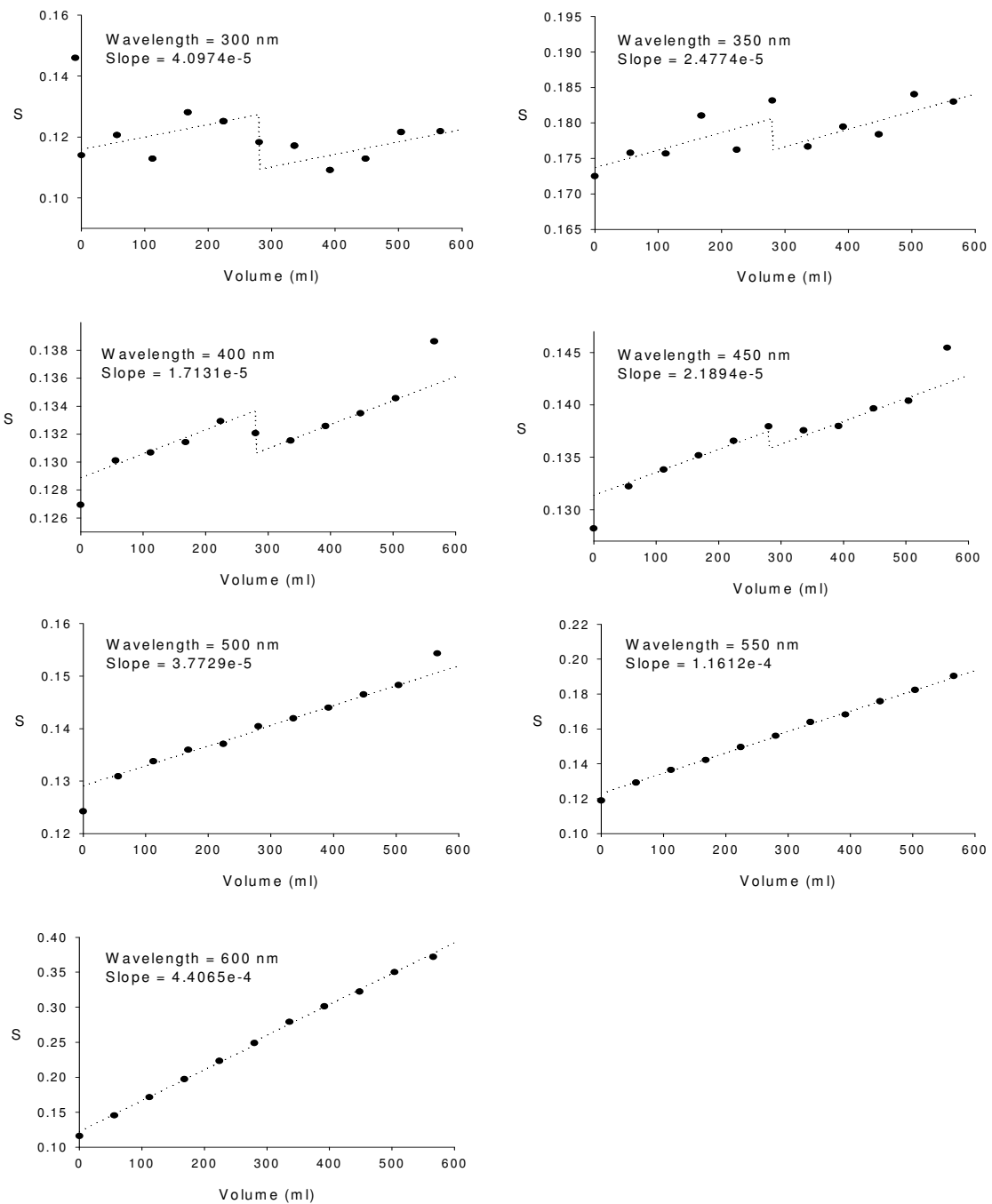
Figure V-5. The ICAM signal *S* as a function of the sample volume *V*

at 7 wavelengths, together with the linear fitting line and slope.
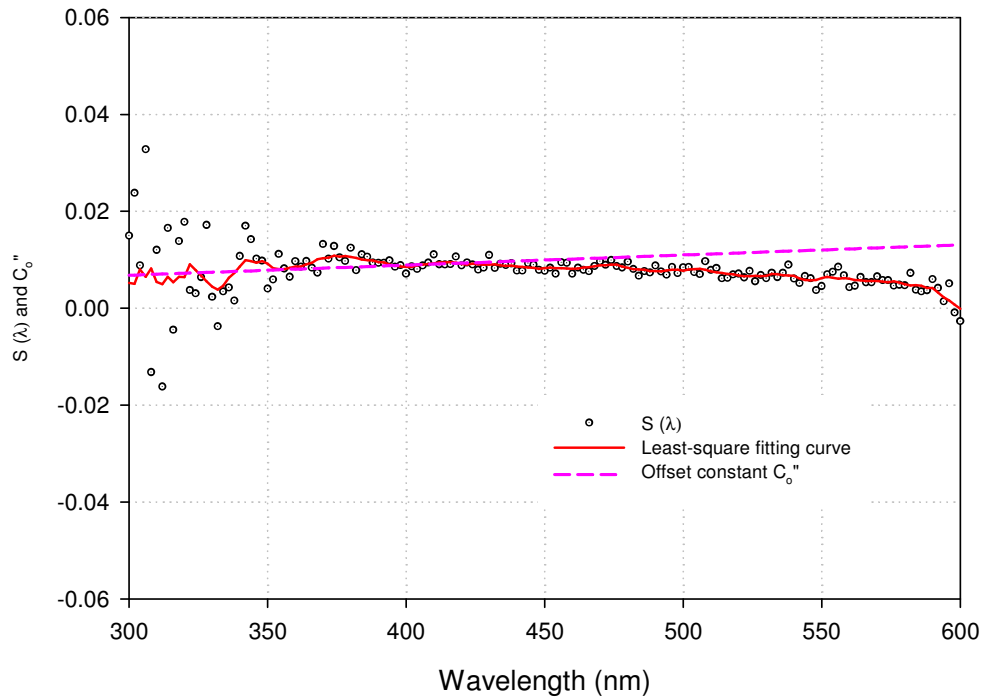
Figure V-6. The net offset $s(\lambda)$. The solid curve is the least-square fit to the data and the dash line is the offset calibration constant C_0''.
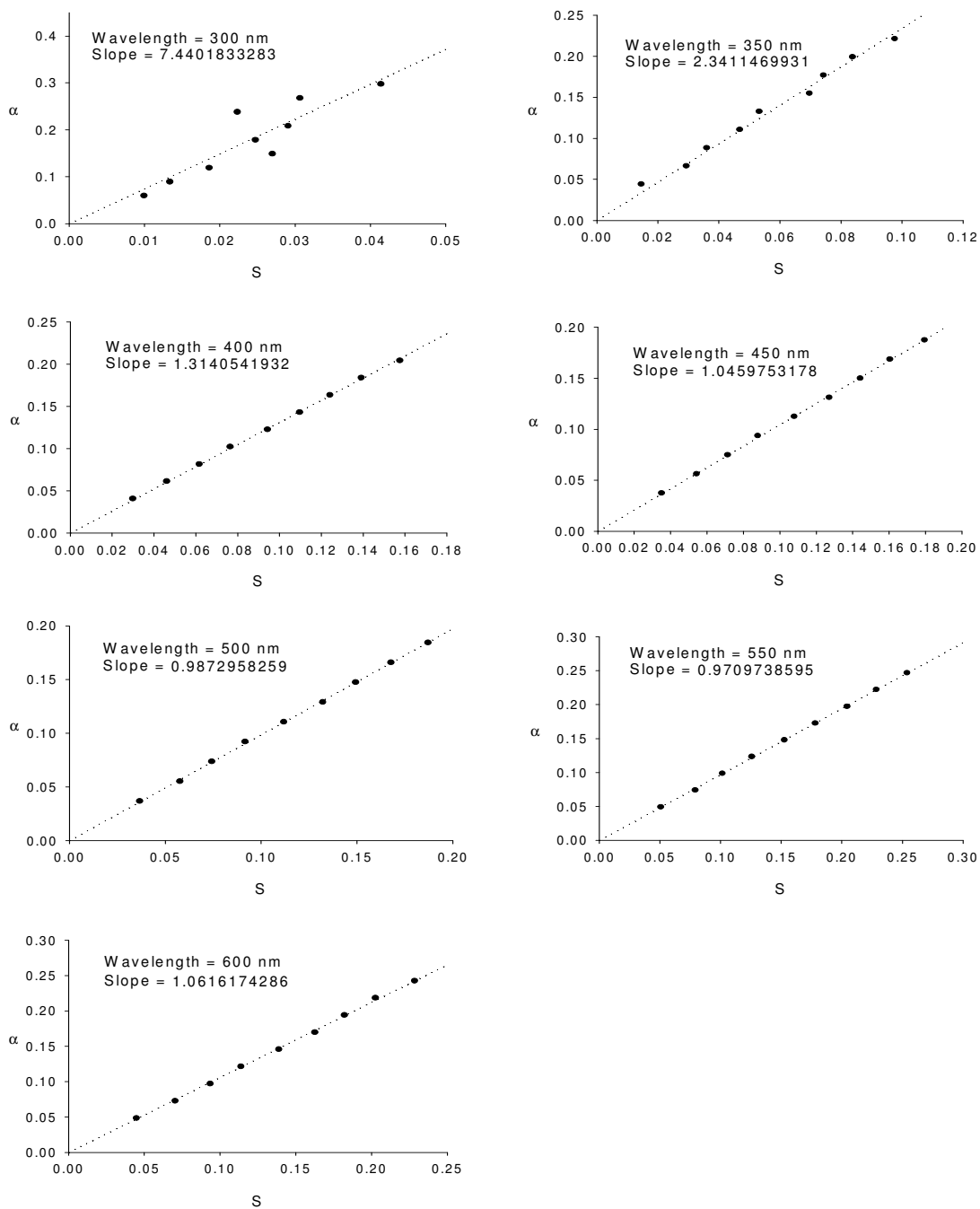
Figure V-7. The absorption coefficient α of the calibration dye solution as a function of the ICAM signal S at 7 wavelengths, together with the linear fitting line and slope.
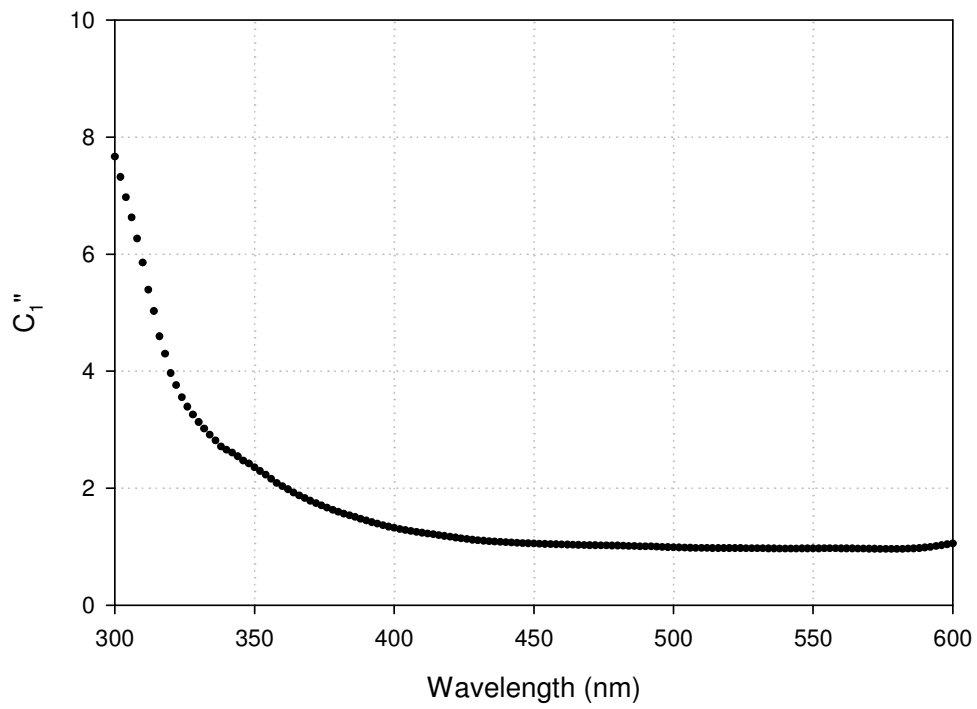
Figure V-8. The normalization constant C_0'' as a function of the wavelength.

5.5 Results

The absorption coefficients of pure water in the range of 300-600 nm are plotted in Fig. V-9. The new data is in good agreement with the work of Pope and Fry[10, 22] in the visible range, as shown in Fig. V-9. It is important to note that these two independent measurements involve completely different diffuse reflecting wall materials: the pressed quartz powder and the Spectralon®. Moreover, the experimental set-up and the measurement procedure are quite different from the previous ICAM: all the optics are UV compatible; new signal detecting and extracting system is implemented; new sample generation and sample delivery system are installed; different calibration dye solution is used; and new data acquisition and instrumental control program is written and used. The values of the absorption coefficients are listed in Table V-1.

Our new data also supports the work of Sogandares and Fry[16, 17]. In their experiment, a different technique using a photothermal probe beam to observe the optical energy deposited as heat in the water sample was applied. The data was taken in 10-nm steps in the range of 340-640 nm.

A comparison with the work of other researchers is shown in Fig. V-10. Comparing the results of Fry's research group (ICAM VERSION-II data, Pope and Fry data, and Sogandares and Fry data) with the Tam and Patel data[53] and the Smith and Baker data[7] shows the significantly lower absorption in the blue. This significant lower absorption in the blue was confirmed by AMANDA research group in South Pole where the deep sea ice samples were measured using pulsed laser[15]. In the UV (300-320 nm) our new data is

higher than Quickenden and Irvin data (subtracted the estimation of the Rayleigh scattering

contribution). [18]

Table V-1. The absorption coefficients of pure water.

Wavelength (nm)	Absorption coefficient (m^{-1})	Wavelength (nm)	Absorption coefficient (m^{-1})
300	0.0504	342	0.0170
302	0.0502	344	0.0161
304	0.0501	346	0.0155
306	0.0467	348	0.0151
308	0.0442	350	0.0150
310	0.0415	352	0.0148
312	0.0388	354	0.0147
314	0.0359	356	0.0145
316	0.0355	358	0.0143
318	0.0354	360	0.0141
320	0.0348	362	0.0141
322	0.0335	364	0.0140
324	0.0325	366	0.0140
326	0.0312	368	0.0140
328	0.0282	370	0.0138
330	0.0256	372	0.0135
332	0.0241	374	0.0136
334	0.0223	376	0.0127
336	0.0208	378	0.0121
338	0.0196	380	0.0115
340	0.0181	382	0.0107

Table V-1. Continued.

Wavelength (nm)	Absorption coefficient (m⁻¹)	Wavelength (nm)	Absorption coefficient (m⁻¹)
384	0.0103	434	0.00585
386	0.00985	436	0.00601
388	0.00913	438	0.00614
390	0.00854	440	0.00645
392	0.00830	442	0.00679
394	0.00776	444	0.00725
396	0.00721	446	0.00773
398	0.00715	448	0.00828
400	0.00691	450	0.00880
402	0.00641	452	0.00922
404	0.00623	454	0.00949
406	0.00596	456	0.00971
408	0.00551	458	0.00989
410	0.00524	460	0.0100
412	0.00502	462	0.0100
414	0.00479	464	0.0103
416	0.00483	466	0.0105
418	0.00471	468	0.0107
420	0.00474	470	0.0110
422	0.00495	472	0.0115
424	0.00496	474	0.0117
426	0.00511	476	0.0120
428	0.00530	478	0.0124
430	0.00543	480	0.0129
432	0.00553	482	0.0130

The absorption coefficient column headers use units of m^{-1}.

Table V-1. Continued.

Wavelength (nm)	Absorption coefficient (m⁻¹)	Wavelength (nm)	Absorption coefficient (m⁻¹)
484	0.0134	534	0.0474
486	0.0138	536	0.0484
488	0.0144	538	0.0496
490	0.0150	540	0.0508
492	0.0160	542	0.0522
494	0.0172	544	0.0539
496	0.0185	546	0.0557
498	0.0199	548	0.0577
500	0.0215	550	0.0597
502	0.0233	552	0.0613
504	0.0253	554	0.0626
506	0.0277	556	0.0638
508	0.0306	558	0.0647
510	0.0338	560	0.0657
512	0.0368	562	0.0667
514	0.0393	564	0.0681
516	0.0411	566	0.0696
518	0.0422	568	0.0714
520	0.0427	570	0.0737
522	0.0430	572	0.0766
524	0.0435	574	0.0801
526	0.0442	576	0.0844
528	0.0448	578	0.0897
530	0.0456	580	0.0964
532	0.0465	582	0.1041

Table V-1. Continued.

Wavelength (nm)	Absorption coefficient (m^{-1})	Wavelength (nm)	Absorption coefficient (m^{-1})
584	0.1131	594	0.1789
586	0.1234	596	0.2004
588	0.1346	598	0.2239
590	0.1471	600	0.2481
592	0.1616		
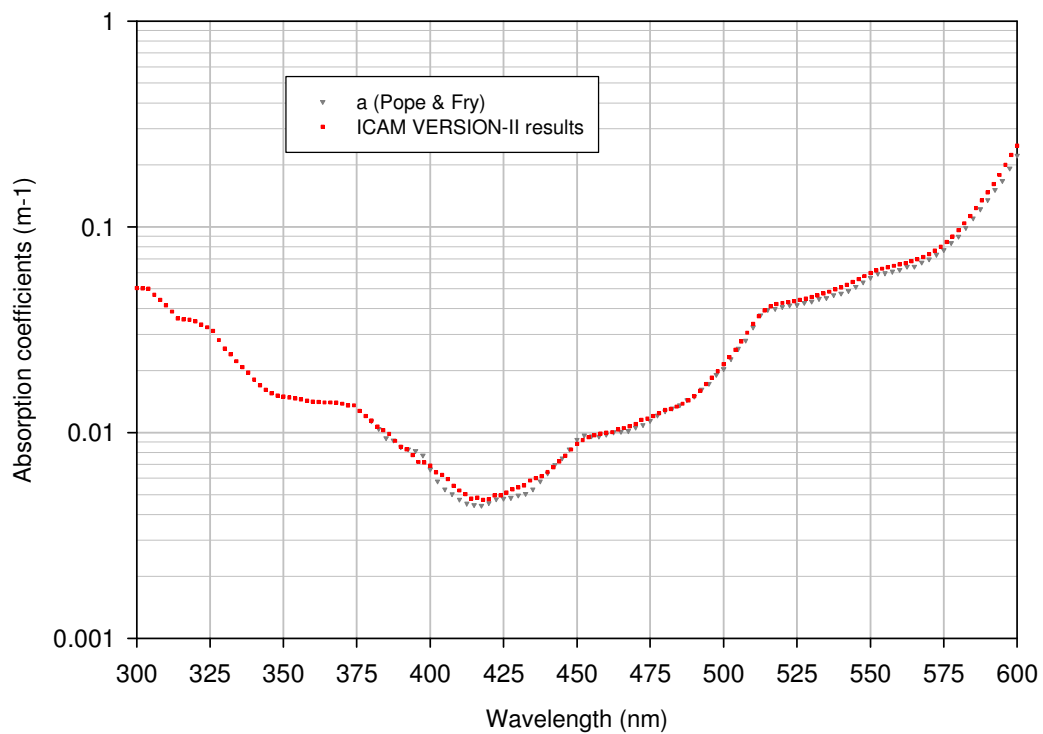
Figure V-9. The absorption coefficient of pure water measured by ICAM VERSION-II, together with Pope and Fry's data.[10,22]

Absorption coefficients (m^{-1})
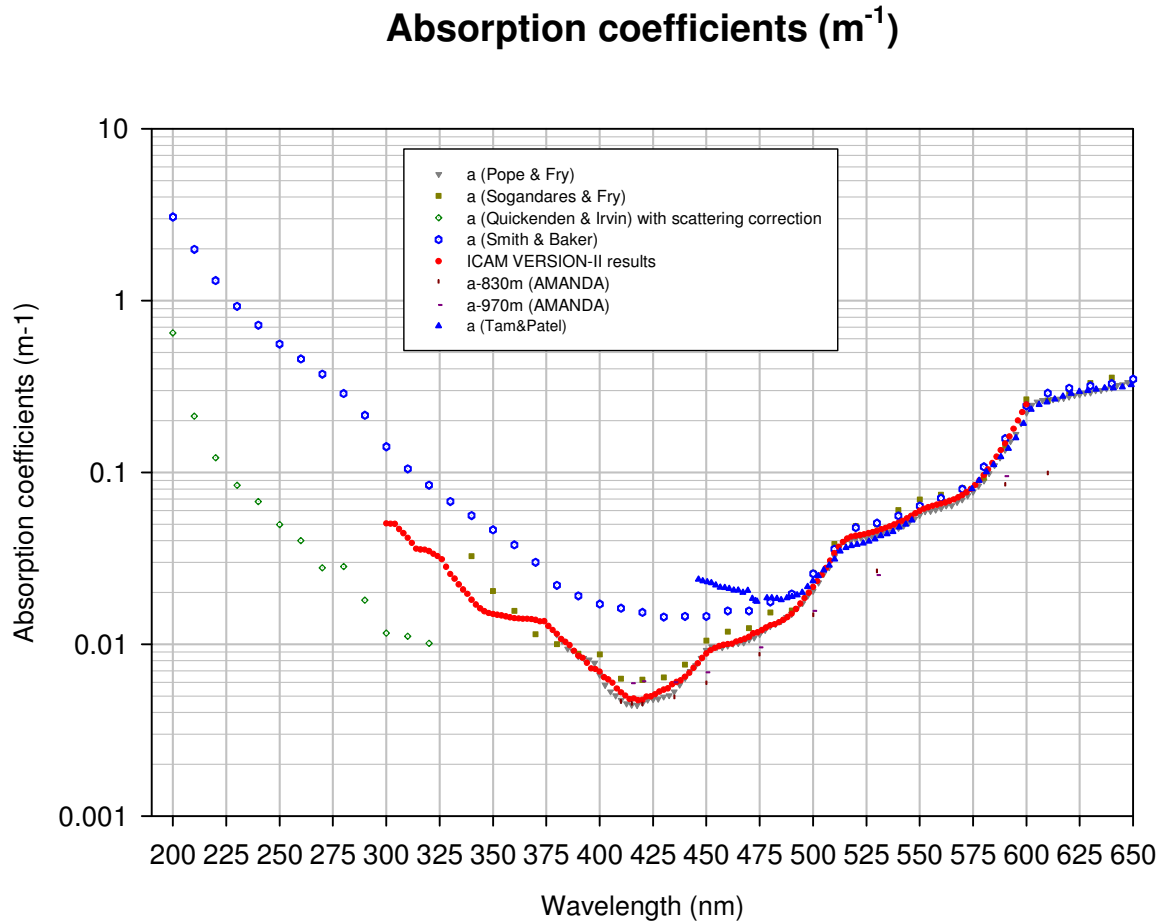
Figure V–10. The absorption coefficient of pure water measured by different groups including Smith & Baker (pure sea water),[7] Quickenden & Irvin,[18] Sogandares & Fry,[16,17] Pope & Fry,[10,22] AMANDA in South Pole where the deep sea ice was measured,[15] and Tam and Patel.[53]

5.6 Resonance Structures

The absorption spectra of pure water identifies the resonance structures (shoulders) due to the harmonic of O-H stretch mode combined with the fundamental of the scissors mode of the water molecule.[10, 22] Fig. V-11 shows the three fundamental vibrational modes of water molecule.

V_1

Symmetric stretch
mode

V_3

Asymmetric stretch
mode

V_2

Scissor mode
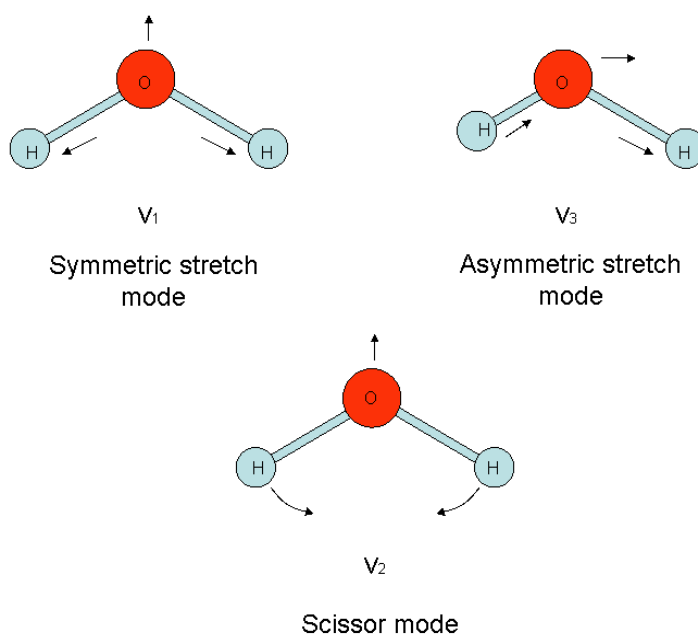
Figure V-11. The fundamental vibrational modes of the water molecule.

The predicated frequencies of the nth harmonic of the O-H stretch mode can be calculated based on the simple anharmonic formula given by Tam and Patel[53]:

$$v_n = n\,(3620 - 63n)\,cm^{-1},\qquad\qquad (5,1)$$

and the frequency of the fundamental scissor mode is 1645 cm^{-1}.

Table V-2 summarizes the vibrational mode assignments with the order of the harmonic of the O-H stretch mode (v_1/v_3) and the scissor mode (v_2); the positions of some predicated shoulders and peaks in the absorption spectra of pure water.

Table V-2. Mode assignments with the predicated wavelengths.

Mode assignments (the order of harmonic)		Predicated shoulder wavelength
v_1/v_3	v_2	λ (nm)
0	1	6079
1	0	2811
4	0	742
4	1	662
5	0	605
5	1	550
6	0	514
6	1	474
7	0	449
7	1	418
8	0	401
8	1	376
9	0	364
9	1	343
10	0	334
10	1	317
11	0	310
11	1	295

Fig. V-12 is another plot of our data to emphasize the resonance structures. Each large arrow with a boldface integer shows the observed shoulder due to the nth harmonic of the fundamental O-H stretch mode. Each small arrow with a pair of numbers in parenthesis shows the minor shoulder due to the conbination modes.

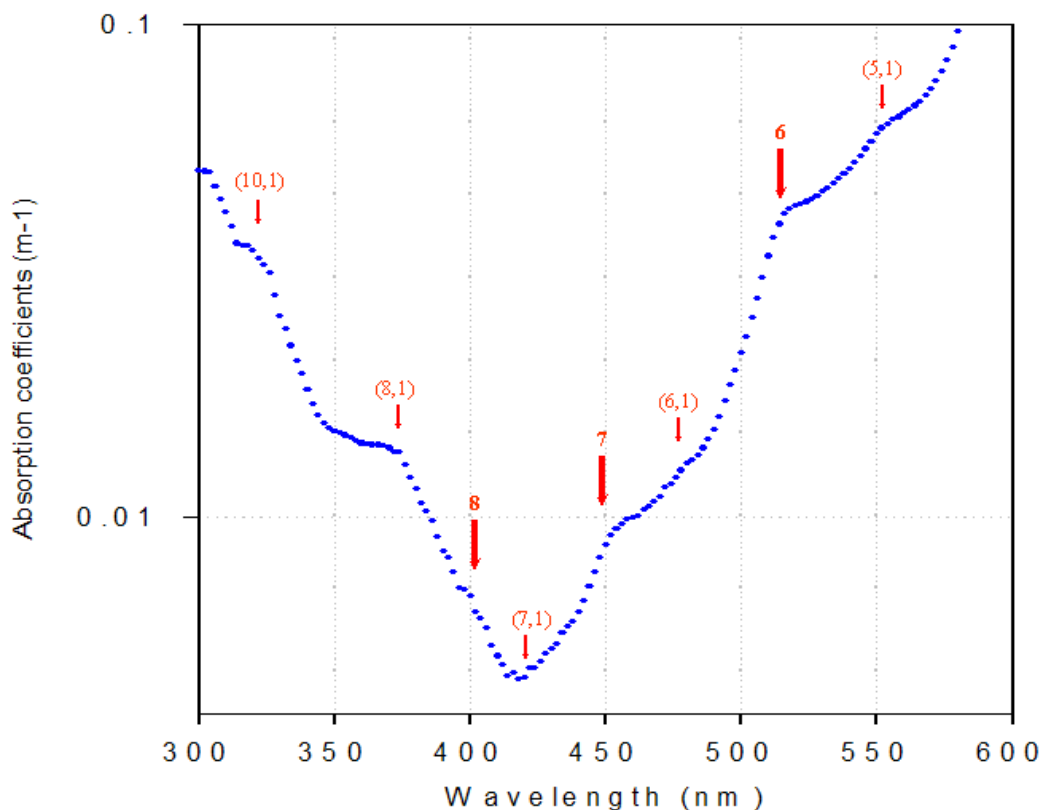**Figure V-12.** The ICAM VERSION-II results for the absorption of pure water. A large arrow with a boldface interger n indicates the position of an oberved shoulder due to the nth harmonic of the O-H stretch mode; a small arrow with mode assignment $(j,1)$ indicates a shoulder due to the combination of the jth harmonic of O-H stretch mode with the fundamental scissors mode.

The shoulders that are due to the seventh and eighth harmonics were first observed by Sogandares and Fry[16, 17] and then confirmed by Pope & Fry,[10,22]. The (7,1) and (6,1) were first observed by Pope & Fry,[10,22] and they have not been readily apparent in water absorption data of other groups. Our new data confirms these shoulders observed by Fry's group in previous work. The (10,1) and (8,1) are two newly observed conbination modes.

5.7 Increased Absorption Due to Long Time Contact of Ultra-pure Water

Pope and Fry[22] observed that the long time contact of ultra-pure water with quartz leaded to significant increased absorption in the blue region. Using ICAM VERSION-II, a fresh pure water sample was measured and then left in the quartz sample cell. Seven days later the sample was measured again with the same experimental setting. During the seven days storage time, the sample was sealed with the high purity nitrogen gas. The measurement result shown in Fig. V-13. indicates the significant increase of absorption of pure water stored in quartz for 7 days in both blue and ultraviolet.

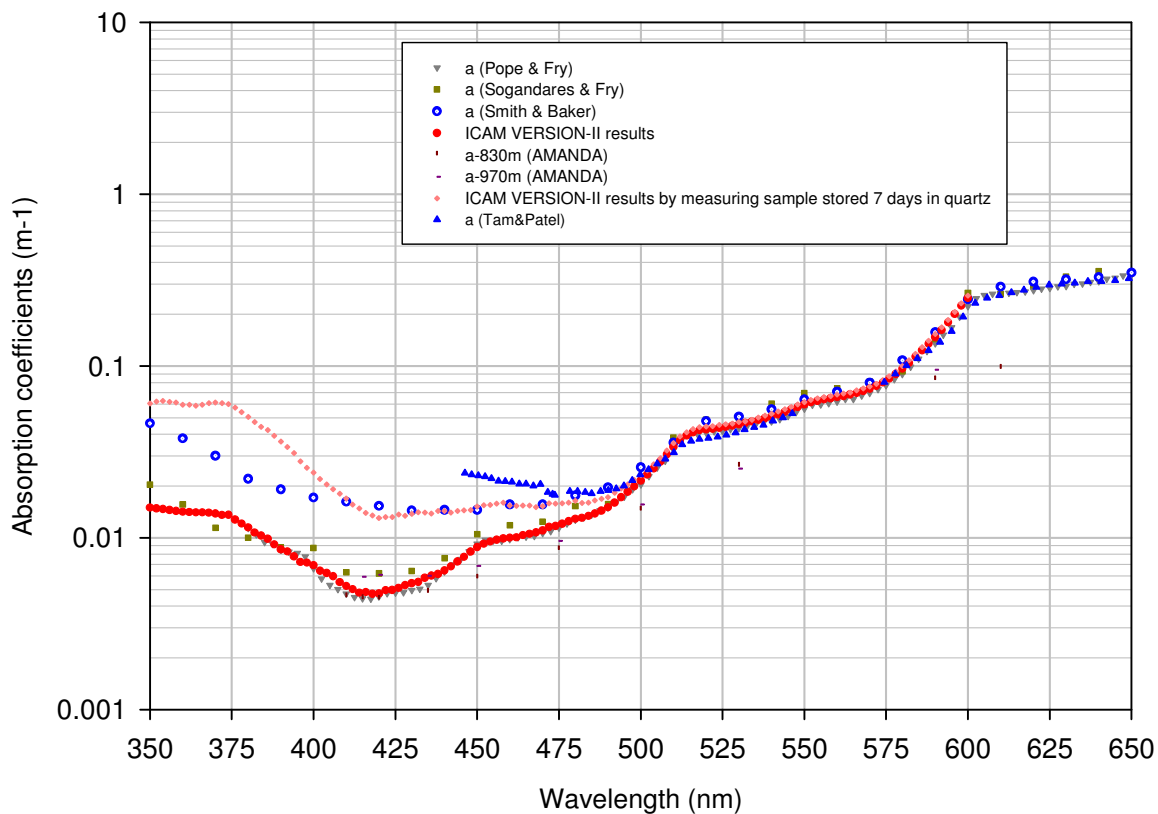## Absorption coefficients (m^{-1})

Figure V-13. Extensive contact of ultra-pure water with quartz leads to increased absorption in the blue and ultraviolet. The result is plotted together with the Smith & Baker data,[7] the Sogandares & Fry data,[16,17] the Pope & Fry data,[10,22] the AMANDA[15], and the Tam and Patel data.[53]

CHAPTER VI

INTEGRATING CAVITY ABSORPTION & SCATTERING METER

Traditionally, the scattering coefficient, b, is obtained by measuring the extinction coefficient, c, the absorption coefficient, a, and using the relation $b=c-a$. This indirect measurement of scattering coefficient can introduce errors in real-world situations. Other techniques involve volume integration of scattering light, which requires mathematical assumptions that may not apply perfectly to real-world situations.

A prototype of an *in situ* device that can directly determine the scattering and absorption of natural water has been studied.[54,55] Fig. VI-1(a) shows the core of this *in situ* device. It consists of two concentric Spectralon® cylindrical cavities with their ends closed by Spectralon® caps and a wavy quaetz tube. The inner Spectralon® cylindrical cavity is lined snuggly by the quartz tube, where the water sample flows. The outer surface of the quartz tube is frosted and the inner surface is polished with sinusoidal features along the cylinder axis. The dimensions labelled in Fig. VI-1(a) are taken as the following: $D_1=13.5$ mm, $D_2=9$ mm, $D_3=7$ mm, $S=50$ mm, and $L=1$ m. The light distribution in the cavities are sampled by optical fibers, and then detected by photodiodes. The fibers are categorized into two groups. The group 1 fibers are used to sample the light in the space where is water sample is. Their ends are placed flush with the inner wall of the inner Spectralon® cavity. The group 2 fibers are used to sample the light in the space between the two Spectralon® cylindrical cavities. Their ends are flush with the inner wall of the outer Spectralon® cavity.
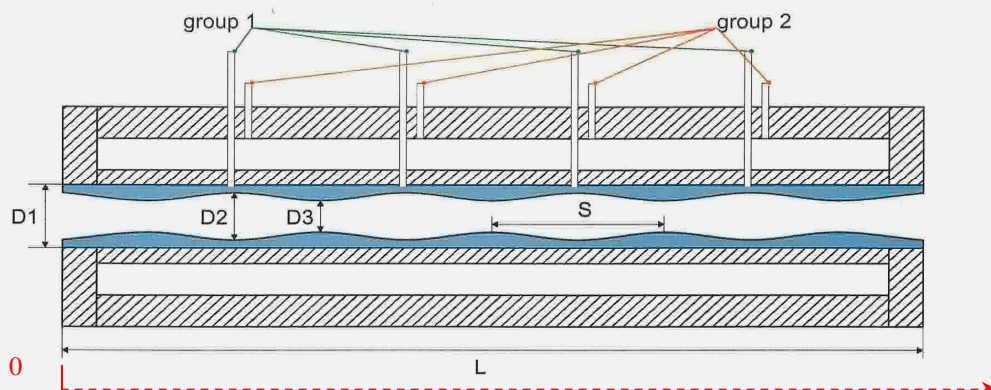
Figure 1(a). Illustration of the wavy quartz tube with the two Spectralon cavities. The two groups of detectors are also shown. The positions of the detectors should not be taken literally, they are placed for illustration purposes only.
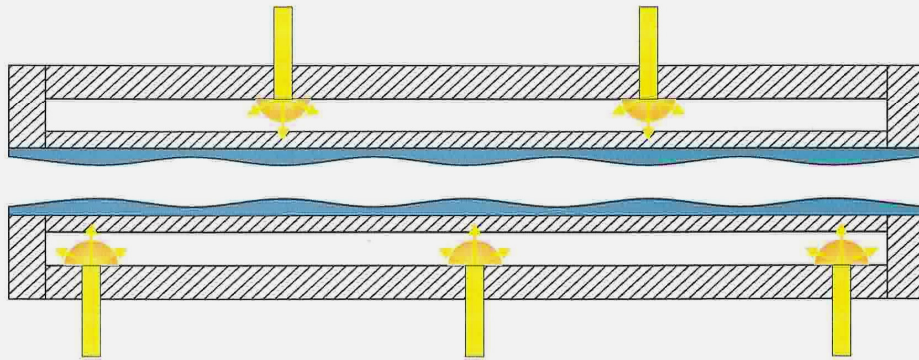
Figure 1(b). The Spectralon illumination mode. The positions of the input fibers are for illustration purposes only.
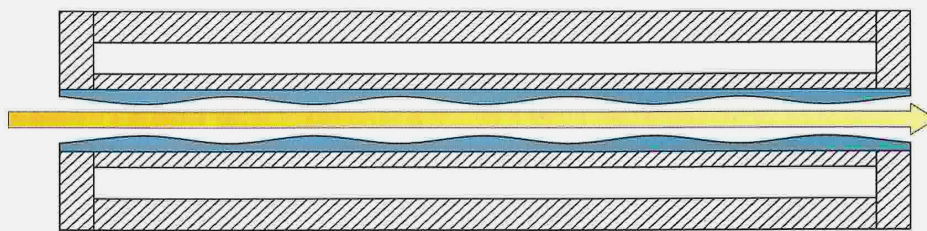
Figure 1(c). The end of illumination mode.

Figure VI-1. Illustration of the *in situ* device that can directly determine the scattering and absorption of natural water.

The introduction of light into the cavity can be achieved in one of the two operating modes: the Spectralon® illumination mode shown in Fig. VI-1(b) and the end illumination mode shown in Fig. VI-1(c). The choice of the mode depends on the optical property of the water to be measured.

To measure the absorption coefficient, the Spectralon® illumination mode is employed. In this mode, light is guided into the space between the inner and outer cavities through optical fibers. The slight translucency of the Spectralon® permits some light penetrate through the wall and enter the space where the quartz tube and the water sample are located. Due to the highly diffuse reflectance of the Spectralon® wall, the sample is under the isotropic and homogeneous illumination. The working principle of the device in this mode is the same as the ICAM VERSION-I and VERSION-II. If absorption is the only property interested, the wavy quartz tube can be replaced by a smooth quartz tube.

To measure the scattering coefficient, the end illumination mode is employed. A well collimated light beam (e.g., a laser beam) is sent down the wavy quartz tube into the water sample along the cylinder axis. It is very important that at no time the beam directly contacts with the inner surface of the quartz tube. The wavy feature of the quartz tube helps prevent the scattered light from escaping so that eventually they reach the detecting fibers. According to the Monte Carlo simulations,[54,55] at a distance of around 0.775 m down the length of cylinder, the detected signal is independent of the $g=0$ and $g=0.97$ phase function, where g is the average cosine of the scattering angle   and phase function is a Henyey-Greenstein phase function given by

$$p(\theta,\phi) = \frac{1}{4\pi}\frac{1-g^2}{(1-2g\cos\theta+g^2)^{3/2}} \ , \ g = \langle\cos\theta\rangle. \tag{6,1}$$

The g=0 case represents isotropic scattering. The g=0 case is chosen to represent a "characteristic upper limit" for real ocean water, in this case most of the scattering light travels forward. The simulation also shows that with a smooth quartz tube, the detected signals are a lot smaller and very different for different g-parameters. The wavy feature of the quartz tube is critical for the measurement of the scattering coefficient. Essentially, in order to measure the scattering coefficient, the best place for the detecting fiber is around 0.775 m from origin shown in Fig. VI-1(a).

The major parts of this *in situ* device shown in Fiu. VI-1(a) have been built. Each of the two Spectralon® cylindrical cavities consists of five tubes. An illustration to show how all the Spectralon® parts are fitted together is shown in Fig. VI-2.
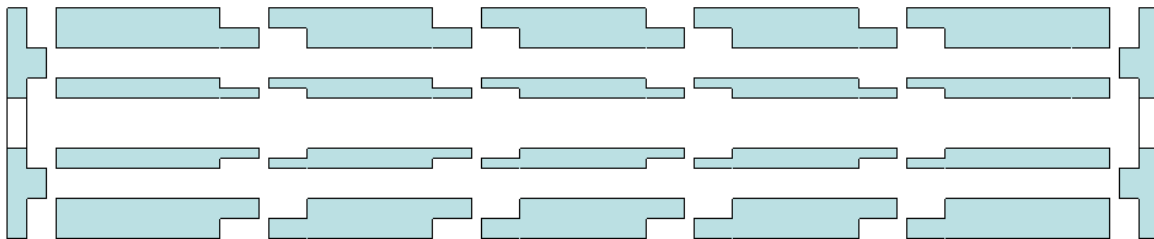
Figure VI-2. An illustration showing how all the Spectralon® parts fit together.

Each outer Spectralon® tube is 20 cm long with a 13.5 mm I. D. and a 21.5 mm O. D.. Each inner Spectralon® tube is 20 cm long with a 32 mm I. D. and a 48 mm O. D.. Each end cap is 8 mm thick with a 13.5 mm I. D. and a 48 mm O. D..

After the major part of the *in situ* device was built, we discovered that the Spectralon® material has absorption and degradation problems. Although the original Spectralon® part is still useful for the measurements of absorption and scattering in the visible region, it will be replaced by the pressed quartz powder in the future studies.

CHAPTER VII

CONCLUSIONS

The results presented in this dissertation indicate the project objectives were achieved. The capability of the Integrating Cavity Absoption Meter (ICAM) was significantly improved to measure the most purified water over the wide spectral range of 300-700 nm. The absorption measurements confirm the results of Pope and Fry in the visible region, specifically in the blue (400-450 nm) where the absorption reaches the the minimum. Besides those resonance structures found in previous work by Sogandares and Pope, some new shoulders were identified in the ultraviolet. As the newly discovered diffuse reflectance material, the pressed fused silica powder was applied to replace the most commonly used Spectralon® material. The integrating cavity based on this new material overcame the low reflectivities in the UV due to cavity wall absorption. The results in this work indicate the pressed quartz powder is very useful in diffuse reflectance spectrophotometry. And it can be used as diffuse reflector for other applications. the fact that the long time contact of ultra-pure water with quartz leads to a significant increase of absorption was observed in both the visible and ultraviolet. The major part of an in *situ device* that can directly measure the scattering and absorption of the natural water was built and under the laboratory test.

Limitations of the current ICAM include the time-consuming calibration process and the corresponding data analysis. New technique based on integrating cavity theory with no (or minimized) calibration efforts will be particularly useful. For example: Fry pointed out that

by measuring the output signal from an empty integrating cavity (made by pressed quartz powder) in response to a very short (in nano-second level) input laser pulse, and comparing the result to the case where the cavity is filled with pure water, it is possible to extract the water absorption information from the laser pulse broading time.

As this dissertation is written, the construction of a new integrating cavity (ICAM VERSION-III) is underway. A smaller quartz sample cell will replace the previous cell so that the quartz powder filling the space between the inner cavity cell and the sample cell will be thicker (currently the thickness of the pressed powder is 5 mm, and it will be increased to 16 mm thickness). This time the powder will be baked overnight together with the inner cavity quartz cell. They will be sealed inside a stainless steel vacuum chamber to prevent the possible contaminants from the oven. During the baking process, a sorption pump will be used to remove the moisture and other organic contaminats in the quartz powder. Once the baking process is completed, the vacuum chamber will be filled with the high purity nitrogen gas.

REFERENCES

[1]   A. Morel, "Optical properties of oceanic Case 1 waters. Revisited," in *Ocean Optics XIII*, S.G. Ackleson and R.Frouin, eds., Proc. SPIE **2963**, 108-114 (1997).

[2]   K. K. Voss, "A spectral model of the beam attenuation coefficient in the ocean and coastal areas," Limnol. Oceanogr. **37**, 501 (1992).

[3]   A. Morel, "Light and marine photosynthesis: A spectral model with geochemical and climatological implications," Prog. Oceanogr. **26**, 263 (1991).

[4]   R. M. Pope, A. D. Weidemann. And E. S. Fry, "Integrating cavity absorption meter measurements of dissolved substances and suspended particles in ocean water," Dynamics of Atmospheres and Oceans **31**, 307-320 (2000).

[5]   H. Buiteveld, J. H. M. Hakvoort, and M. Donze, "The optical properties of pure water," in *Ocean Optics XII*, J. S. Jaffe, ed., Proc. SPIE **2258**, 174-183 (1994)

[6]   M. R. Querry, D. M. Wieliczka, and D. J. Segelstein, "Water (H_2O)," in *Handbook of Optical Constants of Solids II*, E. D. Palik, ed., (Academic Press, Inc., Boston, 1991) pp. 1059-1077.

[7]   R. C. Smith and K. S. Baker, "Optical properties of the clearest natural waters (200-800 nm)," Appl. Opt. **20**, 177-184 (1981).

[8]   W. M. Irvine and J. B. Pollack, "Infrared optical properties of water and ice spheres," ICARUS **8**, 324-360 (1968).

[9]   C. D. Mobley, "The optical properties of water," in *Handbook of Optics*, M. Bass, ed., (McGraw-Hill, New York, 1995) pp. 43.3-43.56.

[10] R. M. Pope and E. S. Fry, "Absorption spectrum (380-700 nm) of pure water: II, Integrating cavity measurements," Appl. Opt. **36**, 8710-8723 (1997).

[11] E. S. Fry and G. W. Kattawar, "Measurement of the absorption coefficient of ocean water using isotropic illumination," in *Ocean Optics IX*, M.A. Blizard, ed., Proc. SPIE **925**, 142-148 (1988).

[12] E. S. Fry, G. W. Kattawar, and R. M. Pope, "Integrating cavity absorption meter," Appl. Opt. **31**, 2055-2065 (1992).

[13]   E. S. Fry, "Visible and near-ultraviolet absorption spectrum of liquid water: comment'" Appl Opt. **39**, 2743-2744 (2000).

[14] E. S. Fry, "Reply to criticisms of the Pope and Fry paper on pure water absorption made in a comment by Quickenden *et al*.," Appl. Opt. **39**, 5843-5846 (2000).

[15]   AMANDA Collaboration, " Optical properties of deep sea ice at the South Pole: absorption," Appl. Opt. **38**, 4168-4180 (1997).

[16] F. M. Sogandares and E. S. Fry, "Absorption spectrum (340-640 nm) of pure water: I. Photothermal measurements," Appl Opt**. 36**, 8699-8709 (1997).

[17] F. M. Sogandares, "The spectral absorption of pure watrer," Ph. D. dissertation (Texas A&M University, College Station, 1991).

[18] T. I. Quickenden and J. A. Irvin, "the ultraviolet absorption spectrum of liquid water," J. Chem Phys. **72**, 4416-4428 (1980).

[19] R. A. J. Litjens, T. I. Quickenden, and C. G. Freeman, "Visible and near-ultraviolet absorption spectrum of liquid water," Appl. Opt. **38**, 1216-1223 (1999).

[20] P. Elterman, "Integrating cavity spectroscopy," Appl. Opt. **9**, 2140-2142 (1970)

[21] J. T. O. Kirk, "Modeling the performance of an integrating-cavity absorption meter: theory and calculations for a spherical cavity," Appl. Opt. **34**, 4397-4408 (1995).

[22] R. M. Pope, "Optical absorption of pure water and sea water using the integrating cavity absorption meter," Ph.D. dissertation (Texas A&M University, College Station, 1993).

[23] L. Cui, "Improved integrating cavity absorption meter," M.S. thesis (Texas A&M University, College Station, 2000).

[24] Millipore Corporation, *A10 Brochure*, Bedford, Mass., 1996.

[25] J. G. Calvert and J. N. Pitts, *Photochemistry* (Wiley, New York, 1966)

[26] High-Q, Inc, *Reagent-Grade Water Newsletter*, issue #0201, (High-Q, Inc., Wilmette, IL., 2002).

[27] Millipore Corporation, *Operating and Maintenance Manual*, (Millipore Corp., Bedford, Mass., 2001).

[28] A. Preece, *A Manual for Histologic Technicians, 3rd ed.*, (Little, Brown & Co., Boston, 1972) pp. 27.

[29] J. Crookham, R. Dapson , *Hazardous Chemicals in the Histopathology Laboratory, 2nd ed.*, (Anatech Ltd., Denver, NC., 1991).

[30] Oriel Instruments, *The Book of Photon Tools*, (Oriel Instruments, Stratford, Conn., 2002).

[31] CVI Laser Corporation, *2004 Catalog*, (CVI Laser Corp., Albuquerque, N.M., 2004).

[32] CVI Laser Corporation, *DIGIKROM 240 Instruction Manual*, (CVI Laser Corp., Albuquerque, N.M., 1988).

[33] CVI Technical Service (800-296-9541), (personal communication, January. 2002).

[34] Labsphere, Inc., *A Guide to Reflectance Coatings and Materials*, (Labsphere, Inc., North Sutton, N. H., 2004).

[35] Labsphere, Inc., *Spectralon® Product Data Sheet*, (Labsphere, Inc., North Sutton, N. H., 2001).

[36] Joan G. Demers, Sr. Technical Sales Representative, (Labsphere, Inc., North Sutton, N. H.) (facsimile transmission 5 May 1989).

[37] EG&G Instruments, *Precision Light Chopper Model 197 User Manual*, (Princeton Applied Research, Oak Ridge, TN, 1999).

[38] Stanford Research System, *SR830 Lock-In Amplifier Operating Manual and Programming Reference*, (Sunnyale, CA, 1999).

[39] EG&G Instruments, *Model 5210 Lock-in Amplifier Instruction Manual*, (Princeton Applied Research, Oak Ridge, TN, 1989).

[40] Life in the Atacama 2005 Science/Technology Workshop, NASA Ames Research Center / Carnegie Mellon, Pittsburgh, PA, 2005.

[41] X. Zhao, Z. Lu and E. S. Fry, "Absorption spectrum (300-700 nm) of pure water using an integrating cavity absorption meter," in *Ocean Optics XVI*, available on CD. from Office of Naval Research, Ocean, Atmosphere, and Space S&T Department, Arlington, VA (2002).

[42] E. S. Fry, Z. Lu, X. Zhao and X. Qu, "Absorption of pure warter in the 300-400 nm range," in *Ocean Optics XVII*, available on CD. from Office of Naval Research, Ocean, Atmosphere, and Space S&T Department, Arlington, VA (2004).

[43] A. E. Stiegmann, C. J. Bruegge and A. W. Springsteen, "Ultraviolet stability and contamination analysis of Spectralon diffuse reflectance material," Opt. Eng. **32**, 799-804 (1993).

 [44] D. R. Gibbs, F. J. Duncan and T. M. Goodman, "Ageing of materials under intense ultraviolet radiation," Metrologia **32** 601-607, (1996).

[45] C. J. Bruegge, A. E. Stiegmann, R. A. Rainen and A. W. Springsteen, "Use of Spectralon as a diffuse reflectance standard for in-flight calibration of earth-orbiting sensors," Opt. Eng. **32**, 805-814 (1993).

[46] E. Hilsenrath, H. Herzig, D. E. Williams, C. J. Bruegge and A. E. Stiegman, "Effects of space shuttle flight on the reflectance characteristics of diffusers in the near-infrared, visible, and ultraviolet regions," Opt. Eng. **33**, 3675-3681 (1994).

[47] P. C. Knee, "Investigation of the uniformity and ageing of integrating spheres," Anal. Chim. Acta **380**, 391-399 (1999).

[48] W Möller, K-P Nikolaus and A. Höpe, "Degradation of the diffuse reflectance of Spectralon under low-level irradiation," Metrologia **40**, S212-S215 (2003).

[49] Bureau Central de la Commission Internationale de l'Eclairage, *Review of Publications on Properties and Reflection Values of Material Reflection Standards*, (CIE Publication 46 (TC-2.3), Paris, 1979) pp. 15-72.

[50] Dr. Gröbel UV-Elektronik GmbH, *Product Catalog*, (Ettlingen, Deutschland, 1980).

[51] V. R. Weidner and J. J. Hsia, "Reflection properties of pressed Polytetrafluoroethylene powder", J. Opt. Soc. Am. **71**, 856-861 (1981).

[52]   Labsphere, Inc., *A Guide to Ingegrating Sphere Radiometry and Photometry*, (Labsphere, Inc., North Sutton, N. H., 2001).

[53] A. C. Tam and C. K. N. Patel, " Optical absorption of light and heavy water by laser optoacoustic spectroscopy," Appl. Opt. **18**, 3348-3358 (1979).

[54] D. J. Gray, G. W. Kattawar, E. S. Fry, and X. Zhao, "Theoretical analysis of a novel in situ scattering and absorption meter," in *Ocean Optics XVI*, available on CD. from Office of Naval Research, Ocean, Atmosphere, and Space S&T Department, Arlington, VA (2002).

[55] E. S. Fry, G. W. Kattawar, D. J. Gray, X. Zhao, and Z. Lu, "Apparatus and method for direct measurement of absorption and scattering coefficient *in situ*," U. S. patent 20040141179A1 (2004).

VITA

Zheng Lu was born in Taiyuan, Shanxi, P.R. China in 1973, to Zhaoying Du and Xingshu Lu. He graduated from the Shandong University in 1996 with a B.S. degree in Optics. In July of 1999 he completed a M.S. degree in Optics from the Institute of Modern Optics at Nankai University. He married Xinmei Qu on 26 July, 1999 and then they came to the United States. They have enjoyed study and research work as graduate students at Texas A&M University. He received his Ph.D. degree in Physics from Texas A&M University in May 2006. His permanent address is 3 Tianwaicun Street, Taishan Sanatorium, Taian, Shandong 271000, P.R.China.